Prediction of Transport Properties of Liquid Ammonia and its Binary Mixture with Methanol by Molecular Simulation

Gabriela Guevara-Carrion[1], Jadran Vrabec*[2], and Hans Hasse[1],

[1] Laboratory for Engineering Thermodynamics, University of Kaiserslautern, Erwin-Schrödinger-Straße 44, 67663 Kaiserslautern, Germany

[2]Thermodynamics and Energy Technology, University of Paderborn, Warburger Straße 100, 33098 Paderborn, Germany

Number of pages: 38

Number of tables: 1

Number of figures: 15

* corresponding author, tel.: +49-5251/60-2421, fax: +49-5251/60-3522, email: jadran.vrabec@upb.de

Abstract

Transport properties of ammonia and of the binary mixture ammonia + methanol are predicted for a broad range of liquid states by molecular dynamics (MD) simulation on the basis of rigid, non-polarizable molecular models of the united-atom type. These models were parameterized in preceding work using only experimental vapor-liquid equilibrium data. The self- and the Maxwell-Stefan diffusion coefficients as well as the shear viscosity are obtained by equilibrium MD and the Green-Kubo formalism. Non-equilibrium MD is used for the thermal conductivity. The transport properties of liquid ammonia are predicted for temperatures between 223 and 473 K up to pressures of 200 MPa and are compared to experimental data and correlations thereof. Generally, a good agreement is achieved. The predicted self-diffusion coefficient as well as the shear viscosity deviates on average by less than 15 % from the experiment and the thermal conductivity by less than 6 %. Furthermore, the self- and the Maxwell-Stefan transport diffusion coefficients as well as the shear viscosity of the liquid mixture ammonia + methanol are studied at different compositions and compared to the available experimental data.

Keywords: Diffusion coefficient; Green-Kubo; Reverse NEMD; Shear viscosity; Thermal conductivity

1 Introduction

In the context of process design in the chemical industry, transport properties essentially determine the equipment size or the operation time scale [1]. However, traditionally, transport data have played a lesser role than other thermodynamic properties like vapor-liquid equilibria. As the need for higher efficiency, process integration and energy awareness in the industry increases worldwide, there is a growing demand for more accurate transport properties [1]. E.g., the area of heat exchangers in catalytic reactors strongly depends on the viscosity and the thermal conductivity of the fluid passing through it [1]. Furthermore, modern rate-based methods for the equipment design and the optimization of distillation or absorption processes require transport coefficient data over a large range of temperature and pressure [2], i.e. diffusivity, thermal conductivity, and shear viscosity [3].

Despite the significant effort devoted to the measurement of transport properties in the last 150 years, accurate experimental techniques were only developed around 1970, the availability of such data is still low [1]. Furthermore, the majority of measurements has been done for simple fluids near ambient conditions of temperature and pressure. Moreover, experimental measurements alone are not able to meet the demand for transport properties from the industry that may comprise several hundred data points for a single process [1]. On the other hand, classical theoretical methods are often unable to accurately predict transport properties of liquids. Hence, there is an increasing interest in the development of better predictive methods. Owing to the rapid increase in computing power, molecular simulation has emerged as a powerful engineering tool for such predictions [4].

Ammonia has a widespread use in many industrial sectors and it is one of the chemicals with the largest production volume in the world. Its main uses are in fertilizers, industrial refrigeration systems, explosives, as well as in plastic and pharmaceutical product manufacturing [5]. Furthermore, ammonia

is often the subject of experimental and theoretical studies, because of its ability to form hydrogen bonds and its simple symmetric molecular structure.

It is not the aim of this contribution to improve a simulation technique, but to show that simple molecular models can reliably be used for the prediction of transport properties in the liquid state. The present work studies the capability of a rigid, non-polarizable molecular model for ammonia, which is computationally efficient [6], to predict the transport properties of greatest importance for the industry, i.e. shear viscosity, thermal conductivity, and diffusion coefficients [1], by molecular dynamics (MD) simulation. This work on ammonia, which is a weakly hydrogen bonding liquid [7], is a continuation of previous successful molecular simulation studies on transport properties of strongly hydrogen bonding liquids: water, methanol, ethanol and their binary mixtures [8, 9].

Along these lines, the self-diffusion coefficient, the shear viscosity, and the thermal conductivity were studied here for ammonia. Furthermore, the self- and the Maxwell-Stefan (MS) diffusion coefficients, as well as the shear viscosity of the mixture ammonia + methanol were assessed. Ammonia was considered to be a chemically stable molecule also in its binary mixture with methanol. These transport properties were predicted in the liquid state over a wide range of thermodynamic conditions. Equilibrium molecular dynamics (EMD) together with the Green-Kubo formalism were used to determine the diffusion coefficients and the shear viscosity. The thermal conductivity was calculated with the reverse boundary driven non-equilibrium molecular dynamics (NEMD) algorithm by Müller-Plathe [10].

The success of MD simulation to predict thermodynamic properties is primarily determined by the molecular model that describes the molecular interactions. Numerous molecular models for ammonia, mostly based on *ab initio* calculations, have been proposed in the literature, e.g. rigid four site [11–13], five site [7, 14, 15], polarizable [16, 17], or flexible models [18–22]. These mod-

els have primarily been employed for studying the microscopic structure and the hydrogen bonding interaction of ammonia, generally not considering other important thermodynamic properties. Accordingly, only a few of these models were assessed with respect to their ability to predict transport properties. For example, the self-diffusion coefficient of liquid ammonia has been predicted on the basis of four models [7, 11, 16, 19, 23] and the shear viscosity only on the basis of a single model [16]. Recently, Feng et al. [23] presented simulation results on the self-diffusion coefficient of ammonia based on a modification of the OPLS-AA model [20]. Their results are very good, however, they used a rather questionable simulation approach, which will be discussed in detail later. Mansour and Murad [16] also found satisfactory results for the self-diffusion coefficient and the shear viscosity based on their polarizable model. To the best of our knowledge, there are no publications on the thermal conductivity of ammonia by MD simulation.

In the case of mixtures containing ammonia, only a few molecular simulation results have been published. Ferrairo et al. [24] predicted the self-diffusion coefficients of water and ammonia in their binary mixture, using the ammonia model by Impey and Klein [7] and the TIP4P [25] water model, and found large deviations to the available experimental data for the pure fluids. Chowdhuri et al. [26] investigated the pressure dependence of the self-diffusion coefficient of ammonia, using the model of Gao et al. [12], when NaCl ions are added. As far as we know, only one molecular simulation study on the mixture ammonia + methanol was published to date: Brink and Glasser [27] employed the Empirical Potential based on the interactions of Electrons and Nuclei (EPEN) to calculate the structure of ammonia-methanol and ammonia-water dimers.

The potential models used in this work for ammonia [28] and methanol [29] were developed in preceding work of our group. Both were optimized to experimental data on vapor pressure and saturated liquid density only. The methanol model exhibits mean unsigned errors compared to experimental data for the vapor pressure, saturated liquid density, and heat of vaporization of 1.1,

0.6, and 5.5 %, respectively, in the temperature range from 280 to 490 K [29]. The ammonia model shows mean unsigned errors compared to experimental data of 0.7 % for saturated liquid density, 1.6 % for vapor pressure, and 2.7 % for the enthalpy of vaporization over the whole temperature range from the triple point to the critical point. Note that no experimental transport property data were taken into account during model parameterization, so that all respective results are strictly predictive.

The outline of the present work is as follows: first, the employed molecular models and the simulation techniques are briefly described. Second, the predictions for self-diffusion coefficient, shear viscosity, and thermal conductivity of pure liquid ammonia are presented and compared to experimental data and correlation equations from the literature. Subsequently, predictions for self- and MS diffusion coefficients as well as the shear viscosity are given for the liquid mixture ammonia + methanol. Finally, conclusions are drawn. The simulation details are summarized in the Appendix.

2 Molecular Models

From the engineering point of view, molecular models should be as simple as possible, but as complex as necessary to yield accurate predictions. Throughout of this work, simple rigid, non-polarizable molecular models of united-atom type from earlier work of our group [28, 29] were used. Both models account for the intermolecular interactions, including hydrogen bonding, by one (ammonia) or two (methanol) Lennard-Jones (LJ) sites and a set of four (ammonia) or three (methanol) superimposed point charges. The potential energy u_{ij} between two molecules i and j can thus be written as

$$u_{ij} = \sum_{a=1}^{n} \sum_{b=1}^{m} 4\epsilon_{ab} \left[\left(\frac{\sigma_{ab}}{r_{ijab}} \right)^{12} - \left(\frac{\sigma_{ab}}{r_{ijab}} \right)^{6} \right] + \frac{q_{ia} q_{jb}}{4\pi\varepsilon_0 r_{ijab}} , \qquad (1)$$

where a is the site index of molecule i, b the site index of molecule j, while n and m are the numbers of interaction sites of molecules i and j, respectively. r_{ijab} represents the site-site distances between molecules i and j. The LJ size and energy parameters are σ_{ab} and ϵ_{ab}. q_{ia} and q_{jb} are magnitudes of the point charges that are located at the sites a and b on the molecules i and j, while ε_0 is the permittivity of the vacuum. The model parameters were taken from [28, 29] and are summarized in Table 1.

The interactions between unlike LJ sites of two molecules were defined by the Lorentz-Berthelot combining rules, which are general practice in the simulation community

$$\sigma_{ab} = \frac{\sigma_{aa} + \sigma_{bb}}{2}\,, \tag{2}$$

and

$$\epsilon_{ab} = \sqrt{\epsilon_{aa}\epsilon_{bb}}\,. \tag{3}$$

In previous work of our group [8, 9], it was shown that these combining rules can be successfully used for predicting transport properties of ideal and highly non-ideal mixtures of hydrogen bonding fluids.

3 Methodology

Transport properties can be obtained from EMD simulations by means of the Green-Kubo formalism [30, 31]. These equations relate a transport coefficient to the time integral of an autocorrelation function of a particular microscopic flux in a system in equilibrium. This method was used here to calculate the self- and the MS diffusion coefficients as well as the shear viscosity. Unfortunately, the autocorrelation function needed to determine the thermal conductivity shows some convergence problems that lead to poor statistics. Therefore,

reverse boundary driven NEMD [10] was applied here in order to overcome these problems.

3.1 Diffusion Coefficients

The Green-Kubo expression for the self-diffusion coefficient D_i is based on the individual molecule velocity autocorrelation function as follows:

$$D_i = \frac{1}{3N_i} \int_0^\infty \mathrm{d}t \, \left\langle \mathbf{v}_i^k(t) \cdot \mathbf{v}_i^k(0) \right\rangle, \tag{4}$$

where $\mathbf{v}_i^k(t)$ is the center of mass velocity vector of molecule k of species i at some time t and $<...>$ denotes the ensemble average. Equation 4 is an average over all N_i molecules of species i in the simulation volume, since all contribute to the self-diffusion coefficient. In a binary mixture, the MS diffusion coefficient $Đ_{ij}$ can also be written in terms of the center of mass velocity [32]

$$Đ_{ij} = \frac{x_j}{3N_i} \left(\frac{x_i M_i + x_j M_j}{x_j M_j} \right)^2 \int_0^\infty \mathrm{d}t \, \left\langle \sum_{k=1}^{N_i} \mathbf{v}_i^k(t) \cdot \sum_{k=1}^{N_i} \mathbf{v}_i^k(0) \right\rangle, \tag{5}$$

where M_i and x_i are the molar mass and the mole fraction of species i.

Because the present simulations provide self- and MS diffusion coefficients simultaneously, a comparison to the simple predictive approach suggested by Darken [33] was possible without any additional simulation effort. Thereby, the MS diffusion coefficient $Đ_{ij}$ is estimated from the self-diffusion coefficients of the two components D_i and D_j in the binary mixture

$$Đ_{ij} = x_i \cdot D_j + x_j \cdot D_i. \tag{6}$$

In previous work on binary mixtures [8, 34], this approach was found to yield good approximations for the MS diffusion coefficient for some mixtures.

3.2 Shear Viscosity

The Green-Kubo formalism associates the shear viscosity η with the time autocorrelation function of the off-diagonal elements of the stress tensor J_p^{xy} [35]

$$\eta = \frac{1}{Vk_BT} \int_0^\infty \mathrm{d}t \, \left\langle J_p^{xy}(t) \cdot J_p^{xy}(0) \right\rangle, \tag{7}$$

where V stands for the molar volume, k_B is the Boltzmann constant, and T denotes the temperature. Averaging over all three independent elements of the stress tensor, i.e. J_p^{xy}, J_p^{xz}, and J_p^{yz}, improves the statistics of the simulation. The component J_p^{xy} of the microscopic stress tensor $\mathbf{J}_p$ is given by [36]

$$J_p^{xy} = \sum_{i=1}^{N} m v_i^x v_i^y - \frac{1}{2} \sum_{i=1}^{N} \sum_{j \neq i}^{N} \sum_{a=1}^{n} \sum_{b=1}^{m} r_{ij}^x \frac{\partial u_{ij}}{\partial r_{kl}^y}. \tag{8}$$

Here, the lower indices a and b count the interaction sites, while the upper indices x and y denote the spatial vector components, e.g. for velocity v_i^x or site-site distance r_{ij}^x. Equations 7 and 8 may directly be applied to mixtures.

3.3 Thermal Conductivity

The thermal conductivity λ characterizes the capability of a substance for molecular energy transport driven by a temperature gradient. In the reverse NEMD simulation method used in this work, a heat flux is imposed onto a molecular system, e.g. in the z direction, and the resulting temperature gradient is measured. For this purpose, the simulation volume is divided perpendicular to the z direction into M slabs of identical thickness L_z/M, where L_z is the length of the simulation volume in the z direction. The slab at $z = 0$ is defined here as the cold slab and the one at $z = L_z/2$ as the hot slab. In order to create a heat flux, the velocity of the molecule with the highest

kinetic energy in the cold slab v_c and the velocity of the molecule with the lowest kinetic energy in the hot slab v_h are interchanged. This mechanism enforces an energy transfer from the cold slab to the hot slab, leading to a temperature gradient. In the steady state, this energy transfer is balanced by the heat flux in the opposite direction that is given by [10]

$$\langle J_c \rangle_t = \frac{1}{2At} \sum_{\text{transfers}} \frac{m}{2} \left(v_h^2 - v_c^2 \right), \tag{9}$$

where A is the cross sectional area in the x and y direction and t is the simulation time.

The temperature gradient ∇T_z is obtained from a linear fit of the temperature profile resulting from the simulation. In the steady state, the thermal conductivity is thus given by

$$\lambda = -\frac{\langle J_c \rangle_t}{\nabla T_z}. \tag{10}$$

4 Simulation Results

The reported values obtained by molecular simulation comprise three different types of error. The statistical uncertainty, which is solely related to sampling, can directly be estimated from the simulation averages and it is documented here for each simulated data point individually. The error introduced by the use of a molecular model, which never behaves exactly as the real fluid, is estimated here by the difference between the predicted and experimental values. This error is given here as the mean deviation for each of the studied properties. The third type of error is introduced by the methodology. This error is expected to be negligible when simulation methods are correctly applied.

4.1 Ammonia

Self-diffusion Coefficient

The self-diffusion coefficient of saturated liquid ammonia was calculated at temperatures between 203 and 330 K and compared to predictions by other authors using different molecular models [7,11,16,19], cf. Fig. 1. The present data show a similar agreement to experimental data than those based on the polarizable ammonia model by Mansour and Murad [16]. The rigid, non-polarizable ammonia models by Impey and Klein [7] as well as by Sagarik et al. [11] strongly underestimate the self-diffusion coefficient. Hannongbua et al. [19], using a flexible model, overestimated this property by about 40 %. Feng et al. [23] did not publish simulation results based on their flexible model for the saturated liquid.

The pressure dependence of the self-diffusion coefficient of ammonia was predicted at 10, 50, 75, 100, 150, and 200 MPa in the temperature range from 203 to 473 K. The full numerical simulation results are listed in Table 1 of the supplementary material. Figure 2 shows, exemplarly, the temperature dependence of the self-diffusion coefficient at selected pressures, i.e. 10, 100, and 200 MPa, in comparison to experimental data by Gross et al. [40]. Consistent with the results at low pressures, i.e. for the saturated liquid states, the predicted self-diffusion coefficient is also underestimated at high pressures. As can be seen in Fig. 2, the deviations increase at high temperatures and pressures, the maximum difference from the experiment is 25 % at 473 K and 200 MPa. Nevertheless, in general, there is a good agreement with the experimental values. The mean deviation is 15 % for the whole range of studied conditions. Moreover, the predicted data correctly cover the temperature dependence of the self-diffusion coefficient for all studied pressures.

Recently, Feng et al. [23] published simulation results for the self-diffusion coefficient over the same temperature and pressure range with apparently better results, using a modification of the OPLS-AA model [20]. Feng et al. [23]

carried out a NpT simulation to determine the density and a subsequent NVT simulation to obtain the self-diffusion coefficient. This is the usual approach that was also used throughout this work. However, Feng et al. [23] did not present numerical values for the density obtained in their simulation runs at specified temperature and pressure (NpT ensemble). In order to obtain this information, the respective simulation runs by Feng et al. [23] were repeated here using the molecular simulation program GROMACS [41] and the obtained density values are rather poor. Exemplarly, Fig. 3 shows the density from the Helmholtz equation of state by Tillner-Roth et al. [42], that is implemented in the database of the National Institute of Standards and Technology (NIST), together with the density data based on the models by Eckl et al. [28] and the modification of the OPLS-AA model [20] by Feng et al. [23] at 50 MPa. Analogous plots at other pressures are given in Figs. 1 to 4 of the supplementary material. It can be seen that the density predicted on the basis of the model used by Feng et al. [23] deviates strongly from the equation of state by Tillner-Roth et al. [42], especially at high temperatures. There, for some state points, the model by Feng et al. [23] even predicts a gaseous state instead of a liquid state. Considering these large differences in density, it is astonishing that the self-diffusion coefficient data reported by Feng et al. [23] agree so well with the experimental values. The reason seems to be the following: In order to calculate the self-diffusion coefficient at temperatures above 332 K, Feng et al. [23] did not use the density from their molecular model, but data from the equation of state by Tillner-Roth et al. [42]. This approach is inconsistent. Furthermore, due to the large deviations for the density, the pressure of the NVT simulations cannot correspond to the state points claimed in [23]. Unfortunately, Feng et al. [23] did not provide any information on the pressure resulting from their NVT simulations.

Shear Viscosity

Figure 4 shows the predicted shear viscosity of saturated liquid ammonia at temperatures between 203 and 330 K. The present simulation results show a similar agreement with experimental data as the predictions by Mansour and Murad [16] using their polarizable model. Because they employed a NEMD method to calculate the shear viscosity, their statistical uncertainties are considerably lower than those of the present results. However, the simulation data by Mansour and Murad [16] are limited to saturated liquid states.

The shear viscosity of liquid ammonia was also predicted at 10, 50, 75, 100, 150, and 200 MPa for temperatures ranging from 203 to 473 K, cf. Table 1 of the supplementary material. The temperature dependence of the shear viscosity is shown in Fig. 5 for three selected pressures together with a correlation of experimental data [43]. Within the statistical uncertainties of around 15 %, the present shear viscosity data agree throughout with the correlation of experimental data, the average deviation is 14 %. At low temperatures and high pressures, the simulation results have larger statistical uncertainties of up to 17 %, which are due to the high density of ammonia under these conditions.

Thermal Conductivity

The thermal conductivity of ammonia was obtained at pressures of 10, 50, 75, 100, 150, and 200 MPa for temperatures ranging from 223 to 473 K, cf. Table 1 of the supplementary material. Figure 6 shows the predicted data at selected pressures in comparison to a correlation of experimental data [44]. As can be seen, the present predictions are in excellent agreement with the correlation; the average deviation is 3 % and the maximum deviation is 6 %. Note that to the best of our knowledge, the thermal conductivity of ammonia was not determined by molecular simulation prior to this work.

4.2 Methanol

In order to discuss transport data for a binary mixture, the performance of both pure fluid models should be assessed. The capability of the methanol model by Schnabel et al. [29] to predict the self-diffusion coefficient, shear viscosity, and thermal conductivity has been discussed extensively in a preceding work [8]. However, only low pressures were considered. Therefore, the temperature dependence of the self-diffusion coefficient and shear viscosity of pure liquid methanol at 50, 100, and 200 MPa was determined here and is shown in Figs. 7 and 8 in comparison to experimental data. As can be seen, a very good agreement with the experiment was found for both studied properties in the entire temperature and pressure range, the average deviations are 9 and 10 % for the self-diffusion coefficient and the shear viscosity, respectively.

4.3 Ammonia + Methanol

Self-diffusion Coefficients

The self-diffusion coefficient of both components in the mixture ammonia + methanol was predicted for 243, 298, and 373 K at 10 and 100 MPa. The simulation results are given in numerical form in Tables 2 and 3 of the supplementary material. Figure 9 shows the present data at 100 MPa in comparison to the experimental data by Gross et al. [47]. The simulation results at 10 MPa are shown in Fig. 5 of the supplementary material.

The predictions by molecular simulation overestimate the self-diffusion coefficient for both ammonia and methanol on average by 25 %. This result is rather unexpected for ammonia, since the self-diffusion coefficient of pure ammonia was underestimated. Unfortunately, the single reported experimental data set for ammonia exhibits significant scatter and does not cover the entire composition range due to experimental problems as reported in [47]. Therefore, the experimental data seem somewhat doubtful, and we refrain from discussing the deviations in more detail.

The experimental self-diffusion coefficient of methanol in the mixture with ammonia deviates from a linear composition dependence, thus the molecular mobility of methanol is smaller than expected for an "ideal solution". This phenomenon has been related to the formation of three-dimensional hydrogen bonding networks of ammonia and methanol molecules in their mixture [47]. The present molecular simulation results indicate only a weak non-ideality of the self-diffusion coefficient for methanol in the studied temperature and pressure range. However, the predicted deviation from the ideal behavior is weaker than that observed experimentally, especially at low temperatures. The higher mobility of the methanol molecules in the present simulations suggests that the hydrogen bonding network formed by the molecular models is weaker than in the real fluid.

Maxwell-Stefan Diffusion Coefficient

The MS diffusion coefficient of the mixture ammonia + methanol was determined for different temperatures and compositions at ambient pressure, cf. Table 4 of the supplementary material. Note that the MS diffusion coefficient at infinite dilution is expected to be the self-diffusion coefficient of the diluted component. In Fig. 10, the predicted values are plotted for different compositions at 313 K and 0.1 MPa, showing that the MS diffusion coefficient is almost constant. The relatively large statistical uncertainties of the direct simulations (14% on average) are attributed to the collective nature of the MS diffusion coefficient. Due to the lack of experimental data, the present simulation data are only compared to Darken's model [33], cf. Eq. 6, based on the self-diffusion coefficients from this work. As can be seen in Fig. 10, Darken's model is consistent with the present direct simulation results.

In Fig. 11, the temperature dependence of the MS diffusion coefficient at 0.1 MPa for $x_{\mathrm{NH3}} = 0.16$ and 0.23 mol/mol is shown. Again, the MS values are compared to Darken's model based on the present self-diffusion coefficients. The agreement is again within the statistical uncertainty. Note

that the consistency of Darken's model cannot be indiscriminately generalized to other systems.

Shear Viscosity

Further simulation runs were performed at conditions for which experimental data for the shear viscosity are available for the mixture ammonia + methanol. Figure 12 shows a comparison of the temperature dependence of the shear viscosity determined by experiment and by simulation for two different compositions of the liquid mixture. As can be seen, the shear viscosity is underestimated by 13 % on average.

Because no experimental data on the shear viscosity of the mixture ammonia + methanol are available at high pressures, the simulation results are compared to the ideal solution model [49]

$$\ln \eta^{\mathrm{id}} = \sum_i x_i \cdot \ln \eta_i, \tag{11}$$

where η^{id} is the shear viscosity of the ideal solution, x_i the molar fraction, and η_i the shear viscosity of the pure fluid i at the temperature and pressure of interest.

Figure 13 shows the calculated ideal solution shear viscosity at 0.1 MPa together with the available experimental data and the present simulation results as a function of the mole fraction of ammonia at 313 K. Note that under these conditions, pure ammonia is gaseous. Therefore, the shear viscosity of the saturated liquid at 313 K was used in Eq. 11.

In Fig. 14, the predicted shear viscosity for the mixture ammonia + methanol at 243, 298, and 373 K and 100 MPa is compared to the shear viscosity of the ideal solution, calculated on the basis of Eq. 11. Similar simulation results obtained at 10 MPa are given in Fig. 6 of the supplementary

material. As can be seen, the present results are in very good agreement with the values for the ideal solution. Hence, the molecular simulation results predict an ideal behavior of the shear viscosity for this mixture. Unfortunately, there are not enough experimental data available to confirm this finding.

5 Conclusion

Transport properties of pure liquid ammonia were predicted at different thermodynamic conditions by MD simulation on the basis of a rigid, non-polarizable molecular model. The self-diffusion coefficient and shear viscosity were calculated by EMD and the Green-Kubo formalism. The thermal conductivity was obtained using reverse boundary driven NEMD. The present self-diffusion coefficient data are in very good agreement with experimental data for temperatures below 350 K for a large pressure range. The self-diffusion coefficient was underestimated at higher temperatures. Simulation results for the shear viscosity were compared to correlations of experimental data and good results were obtained in the regarded temperature and pressure range. The predicted thermal conductivity of ammonia is in excellent agreement with experimental data. In most cases, the chosen simple molecular model performs better than other molecular models from the literature, including computationally more demanding flexible and polarizable models.

Furthermore, the self- and MS diffusion coefficients as well as the shear viscosity of the mixture ammonia + methanol were determined at temperatures from 243 to 373 K and pressures of up to 100 MPa. The composition dependence of the self-diffusion coefficients of both components was well predicted. The MS diffusion coefficient was studied at ambient pressure for three different temperatures. It was shown for the regarded composition range that the present predictions correspond well with Darken's model. The shear viscosity results for the mixture agree well with those expected for ideal solutions.

Acknowledgments

The presented research was conducted under the auspices of the Boltzmann-Zuse Society of Computational Molecular Engineering (BZS). The simulations were performed on the national super computer NEC SX-8 at the High Performance Computing Center Stuttgart (HLRS) and on the HP X6000 super computer at the Steinbuch Center for Computing, Karlsruhe under the grant LAMO. The authors would like to thank Jonathan Walter, Elizabeth Erazo Garzón and Emmanuel Mboo for performing simulation runs.

Appendix Simulation Details

EMD simulations were performed in two steps using the program $ms2$ [50]. In the first step, a simulation in the isobaric-isothermal (NpT) ensemble was performed at the desired temperature and pressure to obtain the density. The system was equilibrated over 8×10^4 time steps followed by a production run of 3×10^5 time steps. In the second step, a canonical (NVT) ensemble simulation was performed at this temperature and density to calculate the transport properties. The simulations in the NpT and the NVT ensemble were carried out in a cubic volume with periodic boundary conditions containing 2048 molecules. Newton's equations of motion were solved using a fifth-order Gear predictor-corrector numerical integrator. The temperature was controlled by velocity scaling. In all simulations, the integration time step was 0.68 fs. The cut-off radius was set to $r_c = 18$ Å. Electrostatic long-range corrections were made using the reaction field technique with conducting boundary conditions ($\epsilon_{RF} = \infty$). On the basis of a center of mass cut-off scheme, the LJ long-range interactions were corrected using angle averaging [51]. The simulations were equilibrated in the NVT ensemble over 10^5 time steps, followed by production runs of $1.5 - 2.0 \times 10^6$ time steps. Diffusion coefficients and shear viscosity were calculated using equations 4 to 7 with up to 10^4 independent time origins of the autocorrelation functions. The sampling length of the autocorrelation functions was between 8 and 12 ps, depending on the thermodynamic conditions. The separation between the time origins was chosen such that all autocorrelation functions have decayed at least to $1/e$ of their normalized value to guarantee their time independence [52]. The statistical uncertainties of the predicted values were estimated by the block averaging method of Flyvbjerg and Petersen [53].

The NEMD simulations for predictions of the thermal conductivity were performed with the YASP simulation package [54]. Here, 1000 molecules were placed in a parallelepiped volume, where periodic boundary conditions were

applied in all directions. The system was equilibrated over 8×10^5 time steps at the desired temperature and pressure by NpT simulation using a weak coupling bath [55] with long-range corrections [56] for pressure and energy. The resulting density of the equilibration run was then taken to generate a new set of simulations in order to develop the thermal gradient in a run of $2.0-3.0\times10^6$ time steps using the NEMD scheme. In this case, the simulation volume was divided into 20 slabs and an exchange frequency of $1/(300$ time steps) for the energy flux was used. Electrostatic interactions were also treated with the reaction field technique with conducting boundary conditions. The thermal conductivity was determined from the average of six different runs. The integration of the equations of motion was performed with a time step of 0.68 fs and a cut-off radius of 15 Å. A Verlet neighbor list was employed to improve the performance of the simulations. An example of a temperature profile obtained using this method is shown in Figure 15.

References

1. W.A. Wakeham, M.J. Assael, *Transport Properties and Industry*, in *Chemical Thermodynamics for Industry*, T.M. Letcher, ed. (The Royal Society of Chemistry, London, 2004)
2. L. Novak, *Int. J. Chem. Reactor Eng.* **9**, A63 (2011)
3. J. Ivakpour, N. Kasiri, *Hydrocarbon Process.* **87**, 75 (2008)
4. E.J. Maginn, J.R. Elliott, *Ind. Eng. Chem. Res.* **49**, 3059 (2010)
5. A. Pearson, *ASHRAE J.* **50**, 30 (2008)
6. C.J. Burnham, S.S. Xantheas, *J. Chem. Phys.* **116**, 1479 (2002)
7. R.W. Impey, M.L. Klein, *Chem. Phys. Lett.* **104**, 579 (1984)
8. G. Guevara-Carrion, C. Nieto-Draghi, J. Vrabec, H. Hasse, *J. Phys. Chem. B* **112**, 16664 (2008)
9. G. Guevara-Carrion, J. Vrabec, H. Hasse, *J Chem. Phys.* **134**, 074508 (2011)
10. F. Müller-Plathe, *J. Chem. Phys.* **106**, 6082 (1997)
11. K.P. Sagarik, R. Ahlrichs, S. Brode, *Mol. Phys.* **57**, 1247 (1986)
12. J. Gao, X. Xia, T.F. George, *J. Phys. Chem.* **97**, 9241 (1993)
13. T. Kristóf, J. Vorholz, J. Liszi, B. Rumpf, G. Maurer, *Mol. Phys.* **97**, 1129 (1999)
14. A. Hinchliffe, D.G. Bounds, M.L. Klein, I.R. McDonald, R. Righini, *J. Chem. Phys.* **74**, 1211 (1981)
15. W.L. Jorgensen, M. Ibrahim, *J. Am. Chem. Soc.* **102**, 3309 (1980)
16. K.A. Mansour, S. Murad, *Fluid Phase Equilib.* **37**, 305 (1987)
17. J.M. Caillol, D. Levesque, J.J. Weis, *Mol. Phys.* **62**, 1225 (1987)
18. M. Diraison, G.J. Martyna, M.E. Tuckerman, *J. Chem. Phys.* **111**, 1096 (1999)
19. S.V. Hannongbua, T. Ishida, E. Spohr, K. Heinzinger, *Z. Naturforsch.* **43a**, 572 (1988)
20. R.C. Rizzo, W.L. Jorgensen, *J. Am. Chem. Soc.* **121**, 4827 (1999)
21. W. Shi, E.J. Maginn, *AIChE J.* **55**, 2414 (2009)
22. C. Engin, T. Merker, J. Vrabec, H. Hasse, *Mol. Phys.* **109**, 619 (2011)
23. H. Feng, X. Liu, W. Gao, X. Chen, J. Wang, L. Chen, H.-D. Lüdemann, *Phys. Chem. Chem. Phys.* **12**, 15007 (2010)
24. M. Ferrario, M. Haughney, I.R. McDonald, M.L. Klein, *J. Chem. Phys.* **93**, 5156 (1990)
25. W.L. Jorgensen, J. Chandrasekhar, J.D. Madura, R.W. Impey, M.L. Klein, *J. Chem. Phys.* **79**, 926 (1983)
26. S. Chowdhuri, D. Chakraborty, A. Chandra, *Indian J. Phys.* **83**, 91 (2009)
27. G. Brink, L. Glasser, *J. Comput. Chem.* **3**, 47 (1982)
28. B. Eckl, J. Vrabec, H. Hasse, *Mol. Phys.* **106**, 1039 (2008)
29. T. Schnabel, A. Srivastava, J. Vrabec, H. Hasse, *J. Phys. Chem. B* **111**, 9871 (2007)
30. M.S. Green, *J. Chem. Phys.* **22**, 398 (1954)
31. R. Kubo, *J. Phys. Soc. Jpn.* **12**, 570 (1957)
32. I.M.J.J. van de Ven-Lucassen, T.J.H. Vlugt, A.J.J. van der Zanden, P.J.A.M. Kerkhof, *Mol. Phys.* **94**, 495 (1998)
33. L. Darken, *AIME* **175**, 184 (1948)
34. G.A. Fernández, J. Vrabec, H. Hasse, *Int. J. Thermophys.* **26**, 1389 (2005)
35. K.E. Gubbins, *Statistical Mechanics*, Vol. 1 (The Chemical Society Burlington house, London, 1972)

36. C. Hoheisel, *Phys. Rep.* **245**, 111 (1994)
37. D.W. McCall, D.C. Douglass, E.W. Anderson, *J. Phys. Chem.* **62**, 1102 (1958)
38. Landolt-Börnstein, *Zahlenwerte und Funktionen*, 5. Teil, Bandteil A (Springer Verlag, Berlin, 1969).
39. D.E. O'Reilly, E.M. Peterson, C.E. Scheie, *J. Chem. Phys.* **58**, 4072 (1973)
40. T. Gross, J. Buchhauser, W. Price, I.N. Tarasov, H.-D. Lüdemann, *J. Mol. Liq.* **73**, 433 (1997)
41. B. Hess, C. Kutzner, D. van der Spoel, E. Lindahl, *J. Chem. Theory Comput.* **4**, 435 (2008)
42. R. Tillner-Roth, F. Harms-Watzenberg, and H.D. Baehr, *DKV-Tagungsbericht* **20**, 167 (1993)
43. A. Fenghour, W.A. Wakeham, V. Vesovic, J.T.R. Watson, J. Millat, E. Vogel, *J. Phys. Chem. Ref. Data* **24**, 1649 (1995)
44. R. Tufeu, D.Y. Ivanov, Y. Garrabas, B. Le Neindre, *Ber. Bunsenges. Phys. Chem.* **88**, 422 (1984)
45. N. Karger, T. Vardag, H.-D. Lüdemann, *J. Chem. Phys.* **93**, 3437 (1990)
46. H.W. Xiang, A. Laesecke, M.L. Huber, *J. Phys. Chem. Ref. Data* **35**, 1597 (2006)
47. T. Gross, L. Chen, J. Buchhauser, H.-D. Lüdemann, *Phys. Chem. Chem. Phys.* **3**, 3701 (2001)
48. M.J.W. Frank, J.A.M. Kuipers, W.P.M. van Swaaij, *J. Chem. Eng. Data* **41**, 297 (1996)
49. J. Kendall, P. Monroe, *J. Am. Chem. Soc.* **39**, 1787 (1917)
50. S. Deublein, B. Eckl, J. Stoll, S.V. Lishchuk, G. Guevara-Carrion, C.W. Glass, T. Merker, M. Bernreuther, J. Vrabec, H. Hasse, *Comput. Phys. Commun.* **182**, 2350 (2011)
51. R. Lustig, *Mol. Phys.* **65**, 175 (1988)
52. M. Schoen, C. Hoheisel, *Mol. Phys.* **52**, 33 (1984)
53. H. Flyvbjerg, H. Petersen, *J. Chem. Phys.* **91**, 461 (1989)
54. F. Müller-Plathe, *Comput. Phys. Commun.* **78**, 77 (1993)
55. H.J.C. Berendsen, J.P.M. Postma, W.F. van Gunsteren, A. Di Nola, J.R. Haak, *J. Chem. Phys.* **81**, 3684 (1984)
56. M.P. Allen, D.J. Tidesley, *Computer Simulation of Liquids*, 2nd edn. (Clarendon, Oxford, 1987)

Table 1. Geometric, Lennard-Jones and point charge parameters of the molecular models for ammonia and methanol, cf. Eq. 1. Boltzmann's constant is k_{B} and the electronic charge is e.

Site	σ Å	$\varepsilon/k_{\mathrm{B}}$ K	q_{ia} e	x Å	y Å	z Å
Ammonia						
$\mathrm{S_N}$	3.376	182.9	−0.9993	0.0	0.0	0.0757
$\mathrm{S_H}$	−	−	+0.3331	0.943	0.0	−0.3164
$\mathrm{S_H}$	−	−	+0.3331	−0.4673	0.8095	−0.3164
$\mathrm{S_H}$	−	−	+0.3331	−0.4673	−0.8095	−0.3164
Methanol						
$\mathrm{S_{CH3}}$	3.7543	120.592	+0.24746	0.7660	0.0134	0.0
$\mathrm{S_{OH}}$	3.0300	87.879	−0.67874	−0.6565	−0.0639	0.0
$\mathrm{S_H}$	−	−	+0.43128	−1.0050	0.8146	0.0

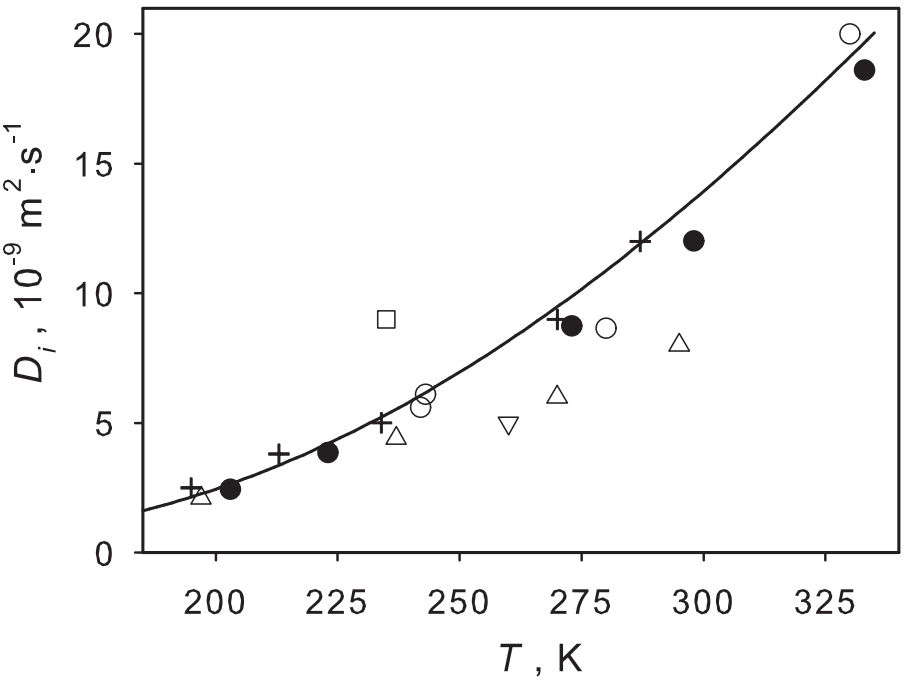

Fig. 1. Temperature dependence of the self-diffusion coefficient of saturated liquid ammonia. Present simulation results (•) are shown together with the predictions on the basis of other molecular models by Impey and Klein [7] (▽), Sagarik et al. [11] (△), Mansour and Murad [16] (○) and Hannongbua et al. [19] (□). Experimental data [37,38] (+) and a correlation thereof [39] (−) are shown for comparison. The statistical uncertainty of the present data is within symbol size.

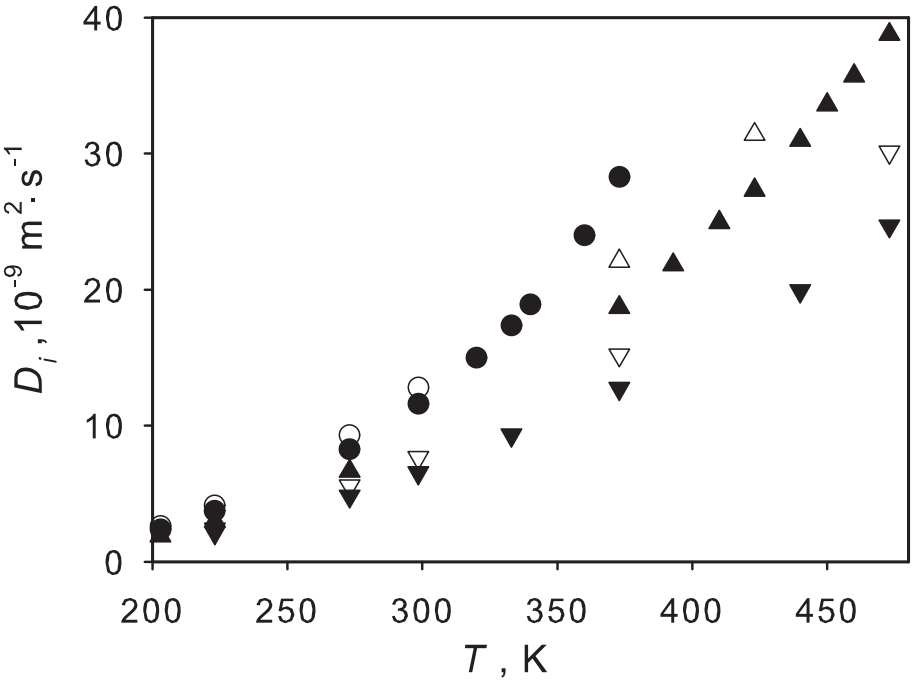

Fig. 2. Temperature dependence of the self-diffusion coefficient of liquid ammonia. Present simulation results at 10 (•), 100 (▲), and 200 MPa (▼) are compared to experimental data [40] (open symbols). The statistical uncertainty of the present data is within symbol size.

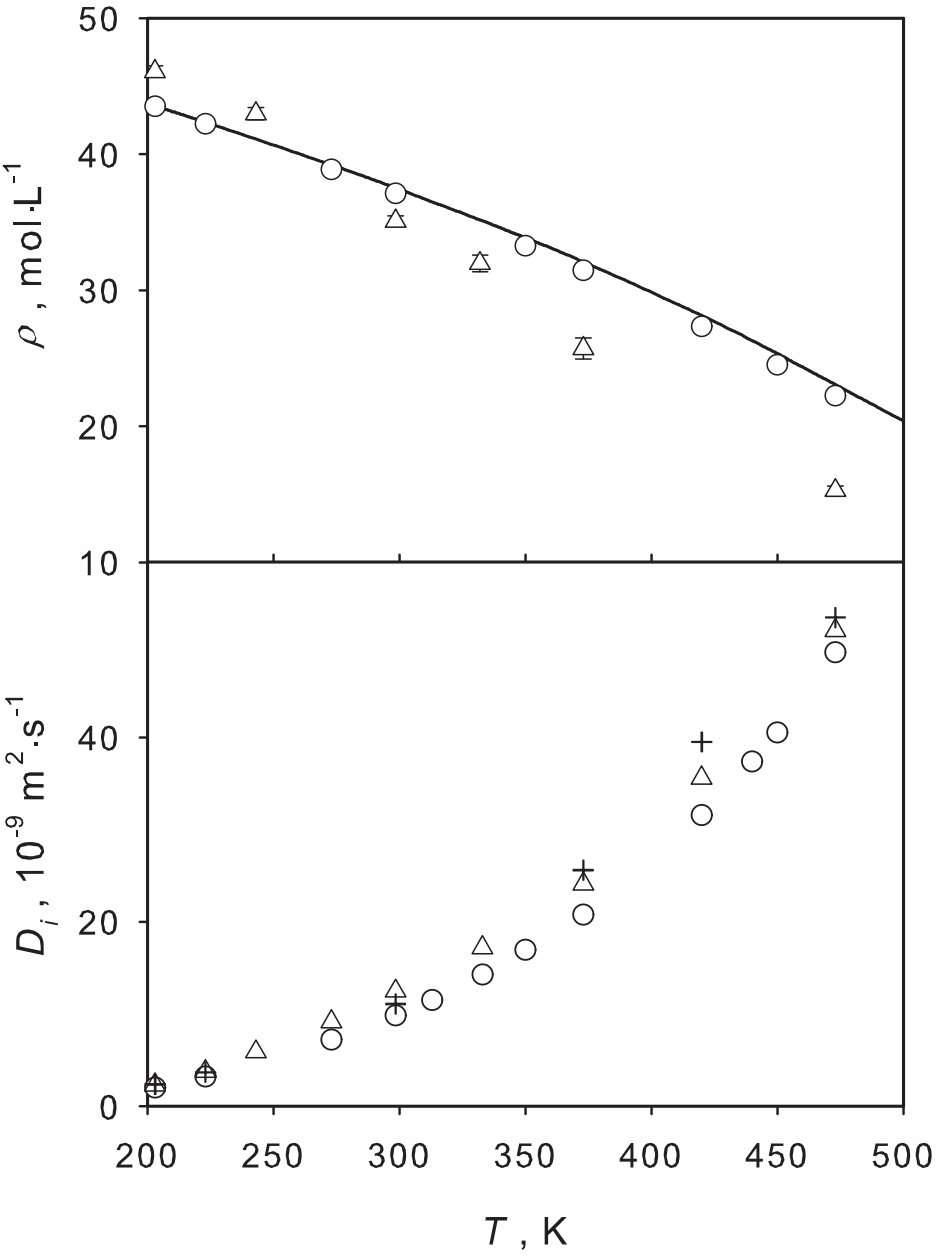

Fig. 3. Top: Temperature dependence of the density of liquid ammonia at 50 MPa. Present simulation results (○) are compared to the simulation results based on the OPLS−AA model modified by Feng et al. [23] (△) and the Helmholtz equation of state by Tillner-Roth et al. (–) [42]. Bottom: Temperature dependence of the self-diffusion coefficient of liquid ammonia at 50 MPa. Present simulation results (○) are compared to the simulation results by Feng et al. [23] (△) and to experimental data [40] (+). The statistical uncertainty of the present data is within symbol size.

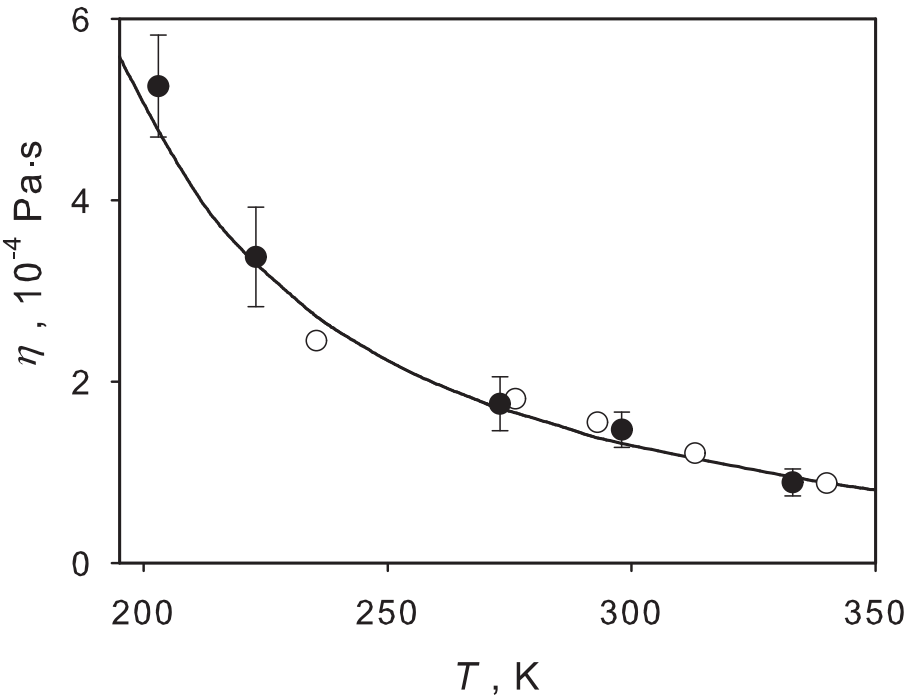

Fig. 4. Temperature dependence of the shear viscosity of saturated liquid ammonia. Present simulation results (•) are shown together with the predictions based on the molecular model by Mansour and Murad [16] (○). A correlation of experimental data [40] (−) is shown for comparison. The error bars indicate the statistical uncertainty of the present data only. Note that Mansour and Murad [16] did not publish the statistical uncertainty of their results.

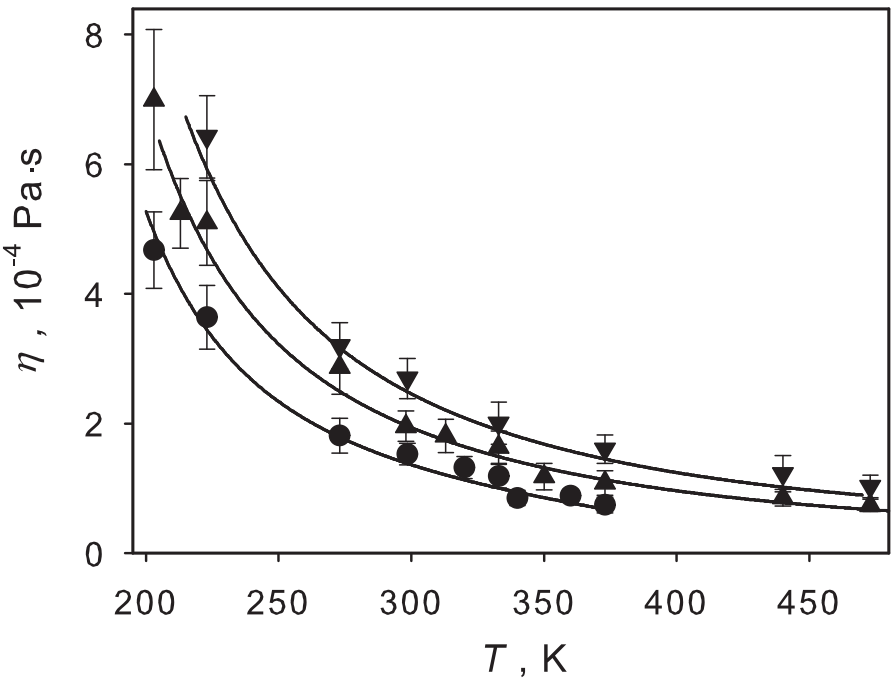

Fig. 5. Temperature dependence of the shear viscosity of liquid ammonia. Present simulation results at 10 (•), 100 (▲), and 200 MPa (▼) are compared to a correlation of experimental data [43] (−). The error bars indicate the statistical uncertainty only.

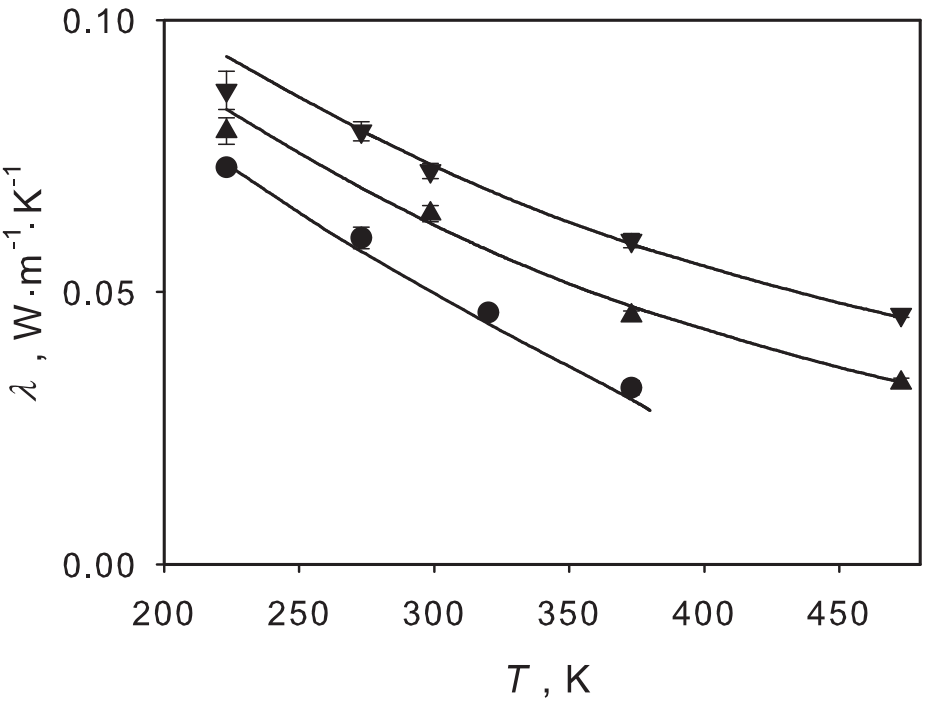

Fig. 6. Temperature dependence of the thermal conductivity of liquid ammonia. Present simulation results at 10 (•), 100 (▲), and 200 MPa (▼) are compared to a correlation of experimental data [44] (−). The error bars indicate the statistical uncertainty only.

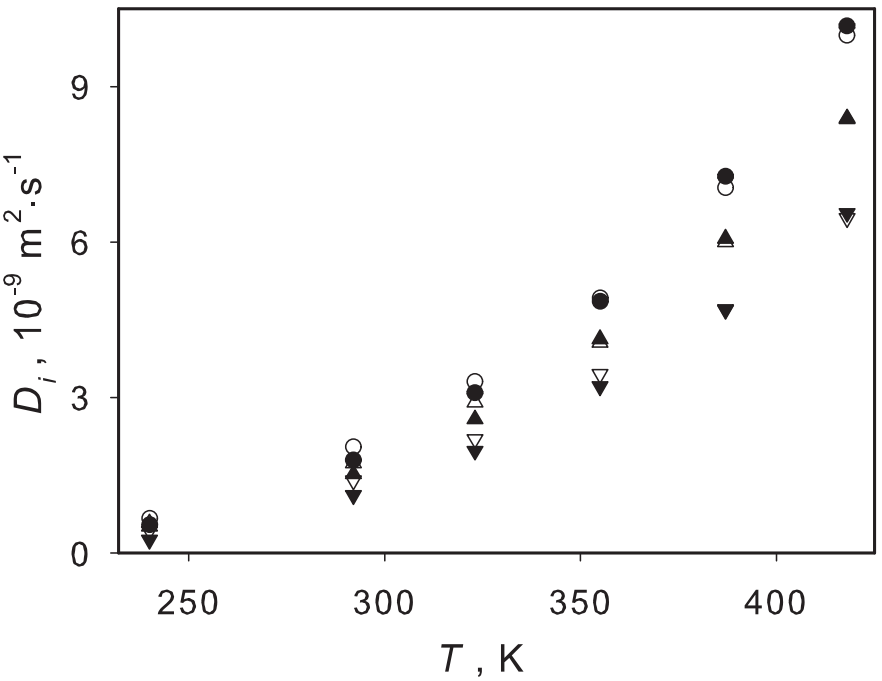

Fig. 7. Temperature dependence of the self-diffusion coefficient of liquid methanol. Present simulation results at 50 (•), 100 (▲), and 200 MPa (▼) are compared to experimental data [45] (open symbols). The statistical uncertainty of present data is within symbol size.

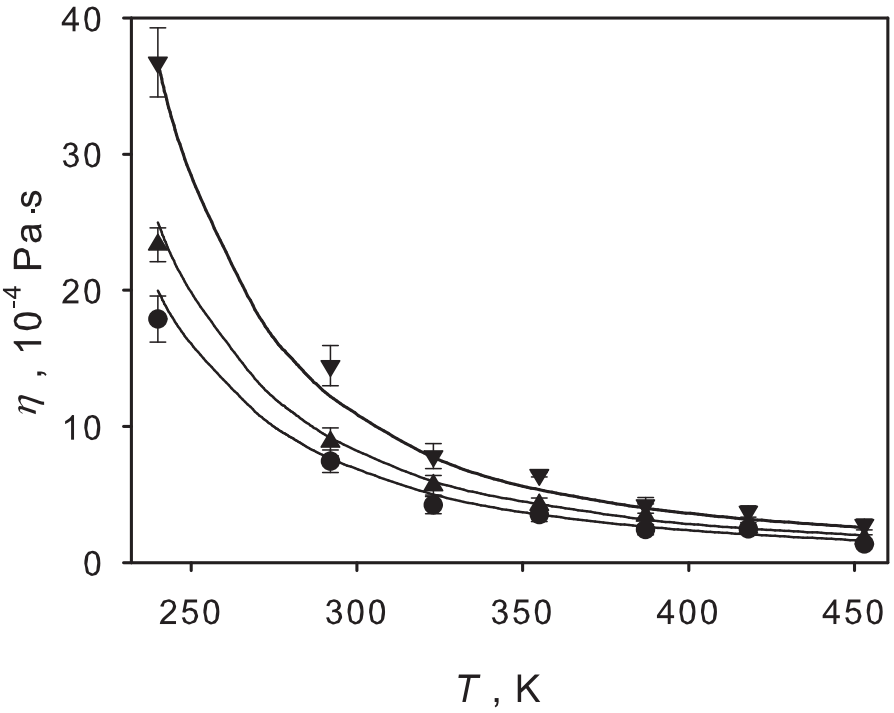

Fig. 8. Temperature dependence of the shear viscosity of liquid methanol. Present simulation results at 50 (•), 100 (▲), and 200 MPa (▼) are compared to a correlation of experimental data [46] (−). The error bars indicate the statistical uncertainty only.

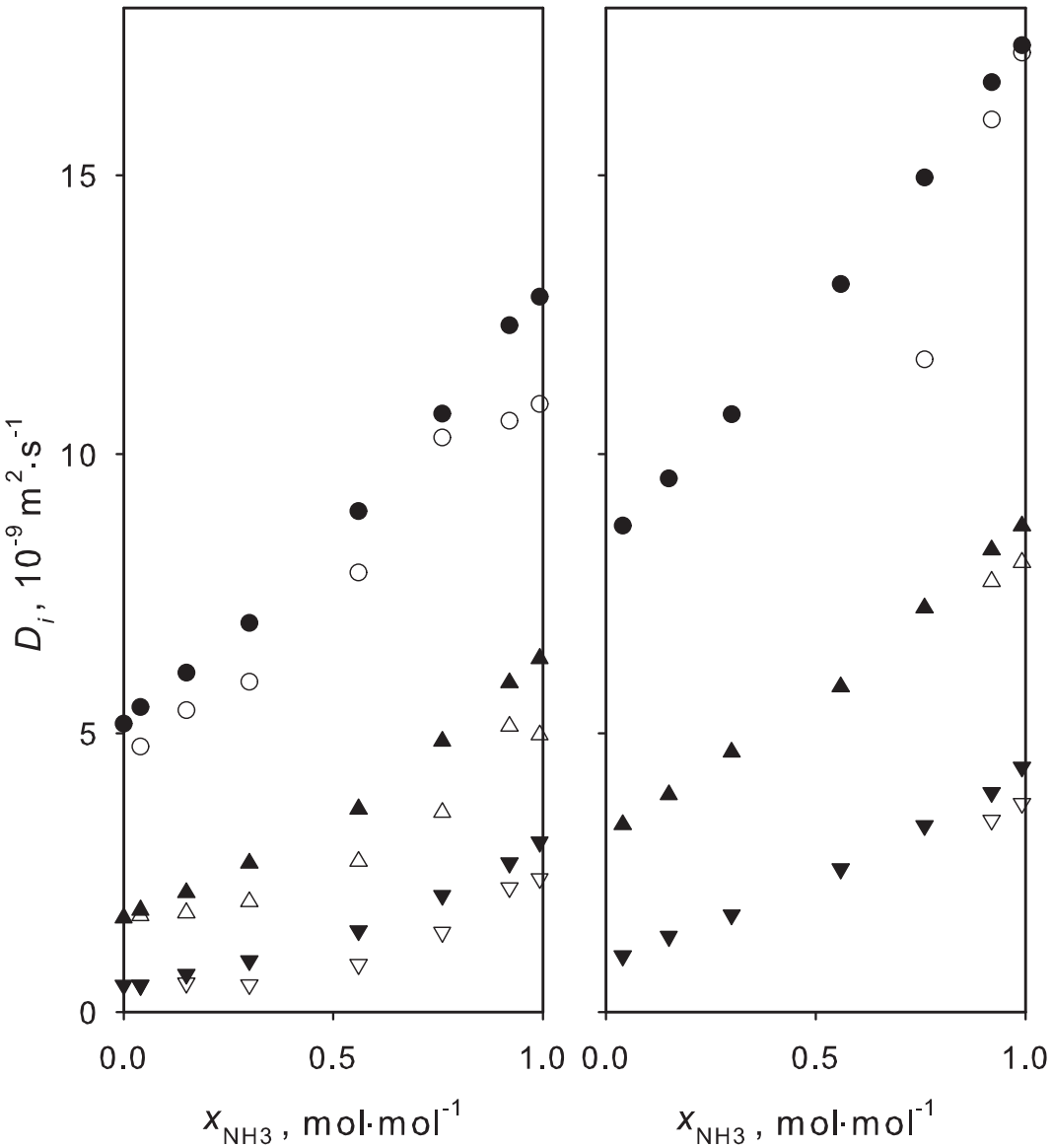

Fig. 9. Composition dependence of the self-diffusion coefficients of ammonia (right) and methanol (left) in their binary liquid mixture at 100 MPa. Present simulation results at 243 (▼), 298 (▲), and 373 K (●) are compared to experimental data [47] (open symbols). The statistical uncertainty of the present data is within symbol size.

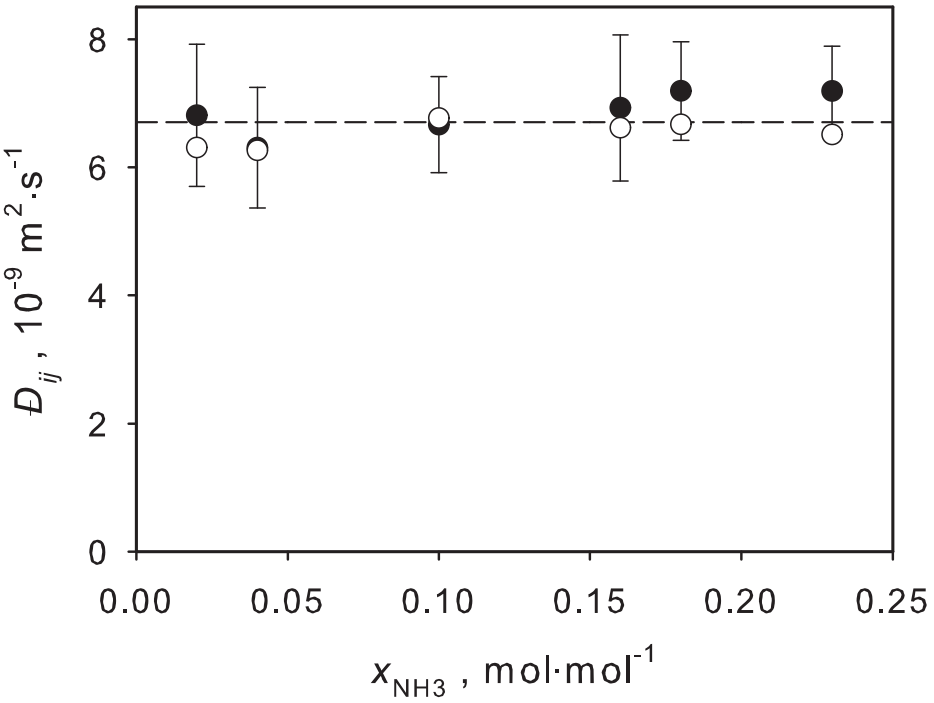

Fig. 10. Composition dependence of the Maxwell-Stefan diffusion coefficient of the mixture ammonia + methanol at 313 K and 0.1 MPa. Present simulation results (•) are compared to Darken's model (○). The horizontal dashed line serves as a guide to the eye. The error bars indicate the statistical uncertainty only.

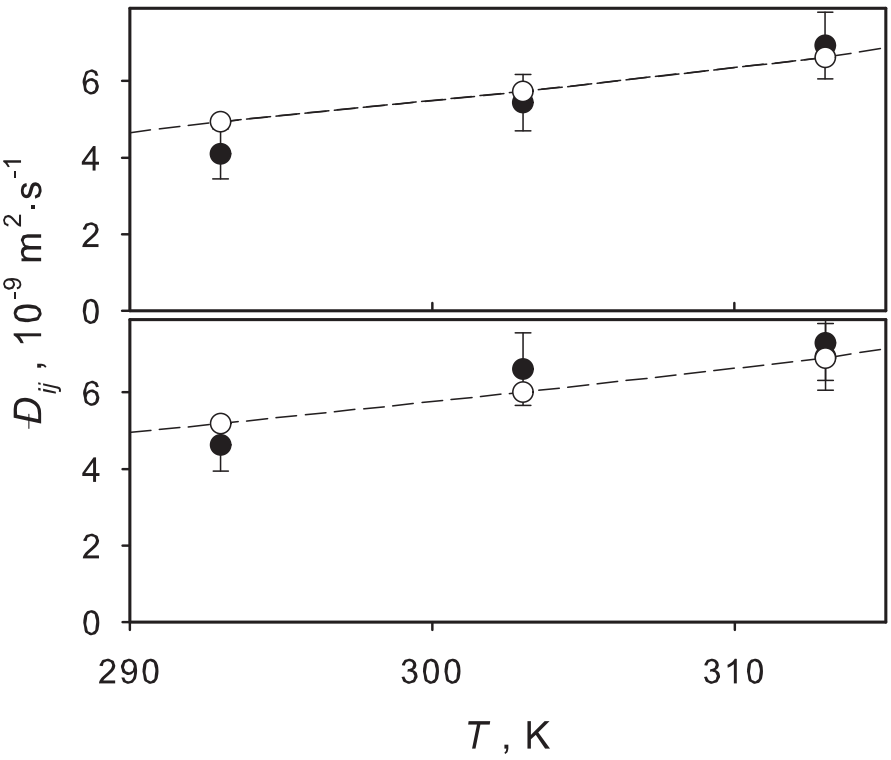

Fig. 11. Temperature dependence of the Maxwell-Stefan diffusion coefficient of the mixture ammonia + methanol at compositions of $x_{\mathrm{NH3}} = 0.16$ mol/mol (top) and 0.23 mol/mol (bottom) at 0.1 MPa. Present simulation results (•) are compared to Darken's model (○). The straight dashed lines serve as a guide to the eye. The error bars indicate the statistical uncertainty only.

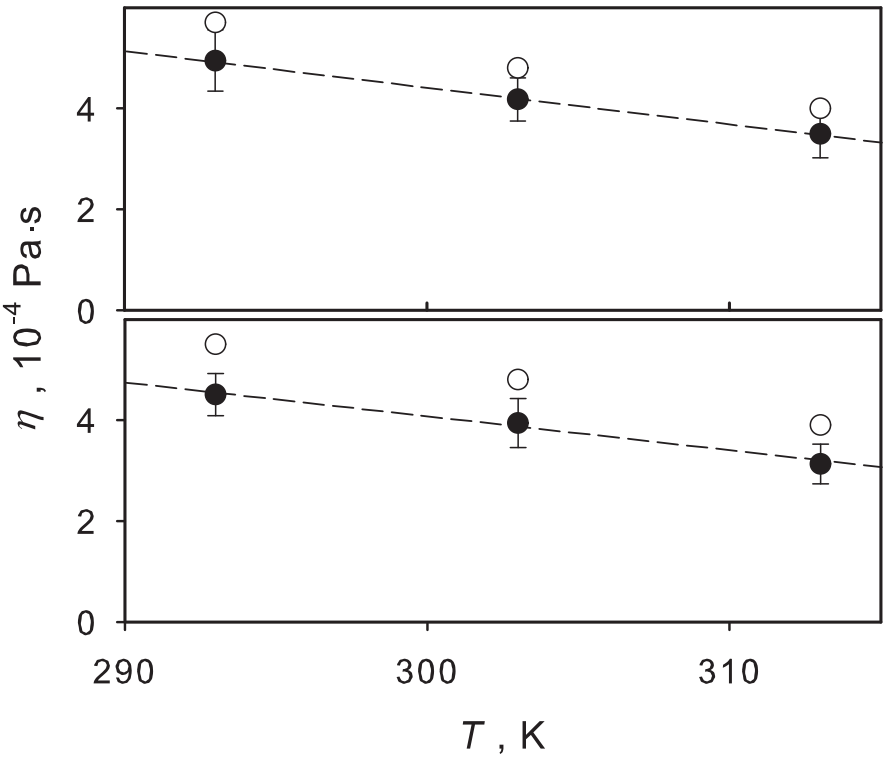

Fig. 12. Temperature dependence of the shear viscosity of the mixture ammonia + methanol at compositions of $x_{\mathrm{NH3}} = 0.16$ mol/mol (top) and 0.23 mol/mol (bottom) at 0.1 MPa. Present simulation results (•) are compared to experimental data [48] (○). The straight dashed lines serve as a guide to the eye. The error bars indicate the statistical uncertainty only.

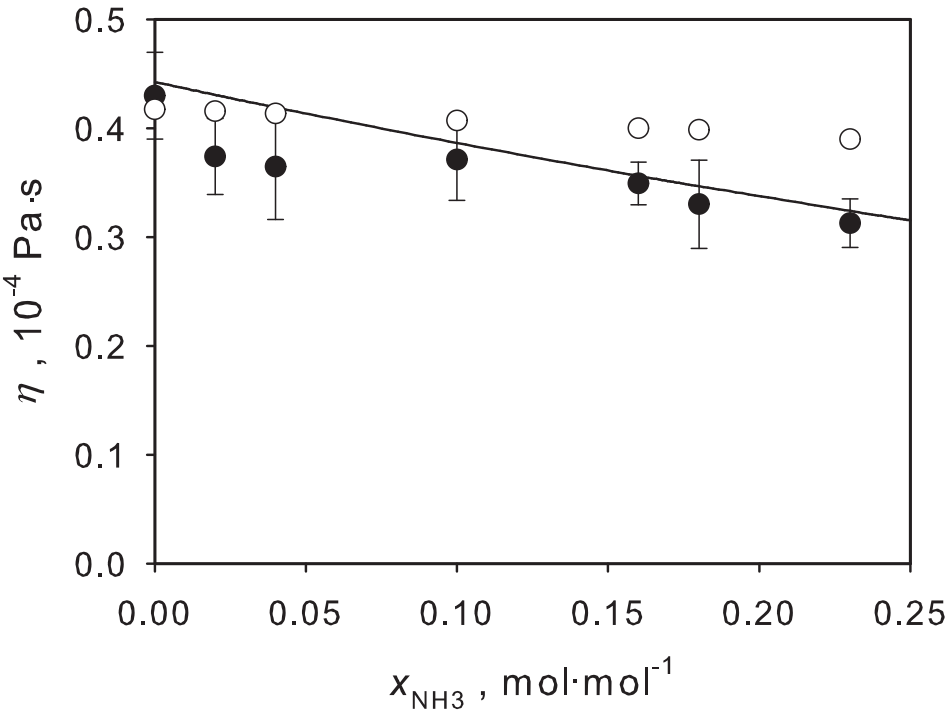

Fig. 13. Composition dependence of the shear viscosity of the liquid mixture ammonia + methanol at 313 K and 0.1 MPa. Present simulation results (•) are compared to the experimental data [48] (○) and the ideal solution shear viscosity (−), based on correlations of experimental data for the pure components [43,46]. The error bars indicate the statistical uncertainty only.

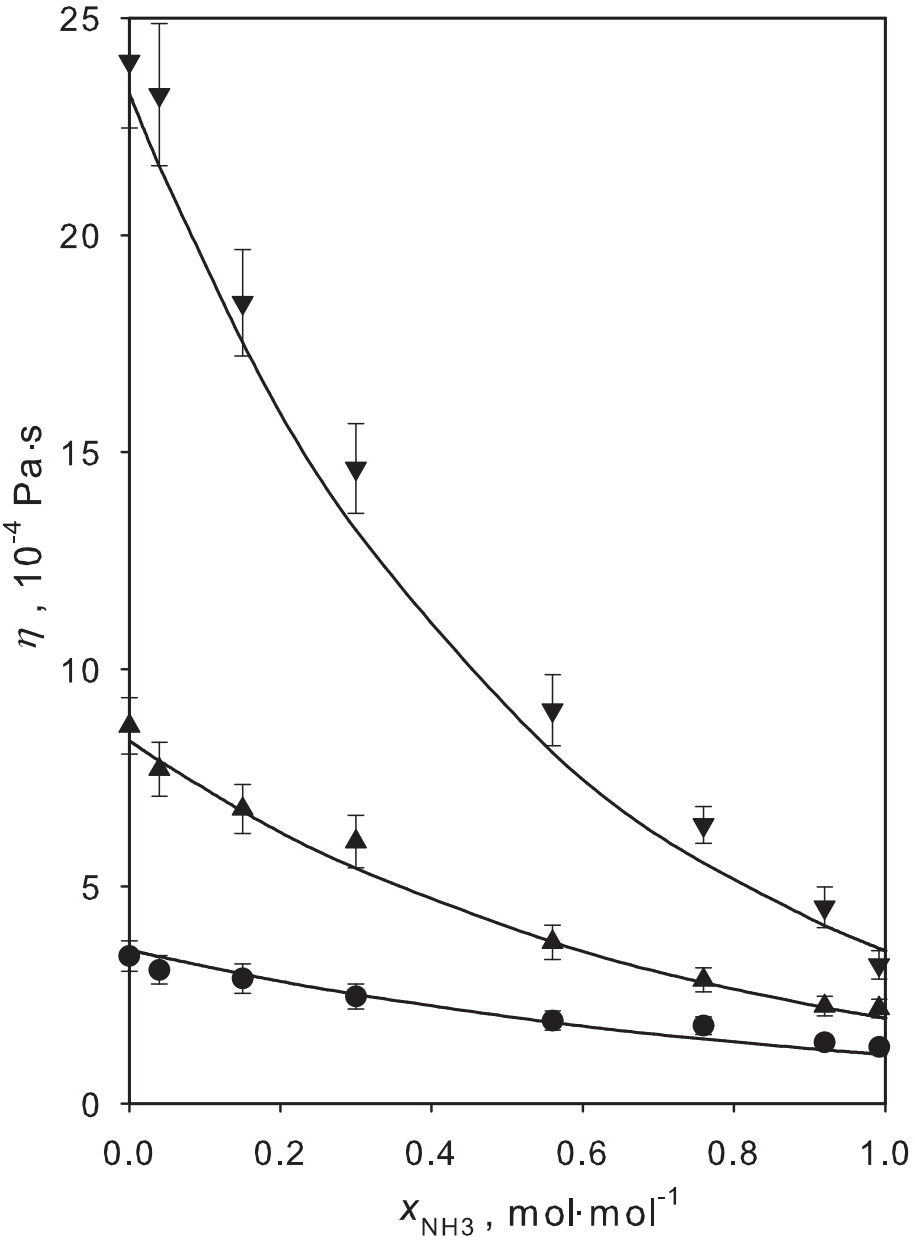

Fig. 14. Composition dependence of the shear viscosity of liquid mixture ammonia + methanol at 100 MPa. Present simulation results at 243 K (▼), 298 K (▲), and 373 K (●) are compared to the ideal solution shear viscosity (−), based on correlations of experimental data for the pure components [43, 46]. The error bars indicate the statistical uncertainty only.

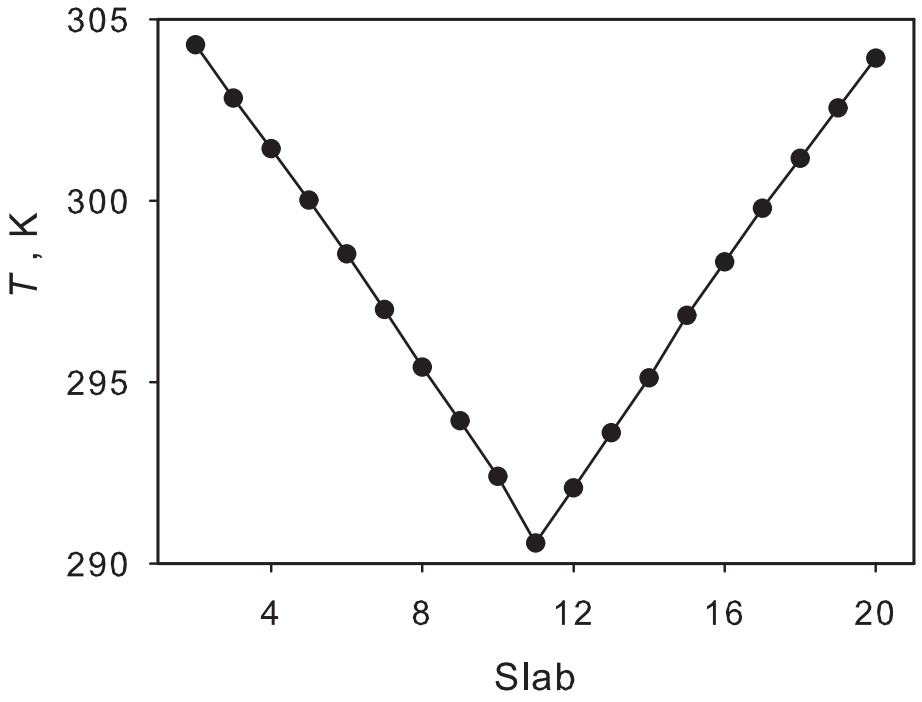

Fig. 15. Temperature profile in the z direction of the NEMD simulation volume for liquid ammonia at 298 K and 10 MPa. The symbols (•) are located at the center of the slabs. The solid lines serve as a guide to the eye.

Supplementary material to: Prediction of the transport properties of liquid ammonia and its binary mixture with methanol by molecular simulation

by

Gabriela Guevara-Carrion, Jadran Vrabec, and Hans Hasse

Table 1. Self-diffusion coefficient, shear viscosity and thermal conductivity of pure liquid ammonia from present NVT simulations. The number in parentheses indicates the statistical uncertainty in the last digit.

T	ρ	D_{NH3}	η	λ
K	mol L^{-1}	10^{-9} m^2 s^{-1}	10^{-4} Pa s	W m^{-1} K^{-1}
10 MPa				
203	42.82	2.30 (2)	5.3 (8)	
223	41.41	3.73 (4)	3.6 (5)	0.73 (1)
273	37.65	8.25 (5)	1.9 (5)	0.60 (2)
298.5	35.51	11.60 (4)	1.5 (2)	
320	33.56	14.98 (5)	1.3 (2)	0.461 (9)
333	32.55	17.36 (7)	1.2 (2)	
340	31.53	18.91 (5)	0.8 (1)	
360	29.16	23.99 (7)	0.9 (1)	
373	27.25	28.3 (1)	0.7 (1)	0.32 (1)
50 MPa				
203	43.52	2.03 (2)	6.8 (9)	
223	42.24	3.22 (2)	4.1 (6)	0.75 (2)
273	38.89	7.19 (3)	2.4 (2)	
298.5	37.12	9.85 (7)	1.7 (5)	0.56 (1)
313	36.37	11.51 (6)	1.6 (2)	
333	34.90	14.29 (7)	1.2 (2)	
350	33.27	16.96 (5)	1.1 (1)	
373	31.47	20.68 (9)	0.9 (1)	0.41 (1)
420	27.35	31.56 (7)	0.78 (9)	
440	25.62	37.4 (1)	0.76 (9)	
450	24.52	40.5 (1)	0.61 (8)	
473	22.26	48.5 (2)	0.51 (9)	0.232 (4)
75 MPa				
203	44.32	1.92 (1)	6.5 (6)	
223	43.10	3.00 (2)	4.7 (5)	0.79 (2)
273	39.92	6.65 (3)	2.3 (3)	
298.5	38.25	9.06 (4)	2.0 (3)	0.61 (2)
373	32.90	18.7 (1)	1.0 (2)	0.45 (1)
393	31.50	21.82 (6)	1.1 (1)	
410	30.27	24.93 (6)	0.9 (1)	
423	29.33	27.3 (1)	0.9 (2)	
440	28.31	30.97 (7)	0.71 (8)	

Continued on next page

Table 1 – continued from previous page

T	ρ	D_{NH3}	η	λ
K	mol L^{-1}	10^{-9} m^2 s^{-1}	10^{-4} Pa s	W m^{-1} K^{-1}
450	27.34	33.5 (1)	0.70 (7)	
460	26.61	35.70 (9)	0.62 (9)	
473	25.69	38.8 (1)	0.6 (1)	0.297 (9)
100 MPa				
203	44.32	1.69 (1)	7.3 (9)	
223	43.12	2.78 (2)	5.1 (6)	0.80 (2)
273	40.15	6.27 (4)	3.0 (4)	
298	38.92	8.41 (3)	2.0 (2)	0.64 (2)
313	38.02	9.89 (5)	1.8 (2)	
333	36.81	11.97 (6)	1.7 (2)	
350	35.45	13.87 (6)	1.2 (2)	
373	34.01	16.80 (7)	1.1 (2)	0.457 (9)
440	29.84	27.45 (9)	0.8 (1)	
473	27.79	33.4 (1)	0.64 (9)	0.333 (8)
150 MPa				
203	45.00	1.44 (1)	7.2 (9)	
223	43.90	2.39 (2)	5.0 (6)	0.82 (6)
273	41.15	5.50 (2)	2.8 (3)	
298.5	39.78	7.32 (4)	2.5 (3)	0.67 (3)
313	39.33	8.63 (5)	2.1 (3)	
333	37.90	10.43 (5)	1.5 (2)	
373	35.77	14.37 (6)	1.4 (2)	0.534 (8)
440	32.27	22.85 (8)	1.0 (2)	0.39 (1)
473	30.63	27.68 (9)	0.9 (1)	
200 MPa				
223	44.59	2.10 (1)	6.43 (6)	0.87 (4)
273	42.05	4.81 (2)	3.6 (4)	0.80 (2)
298.5	40.76	6.53 (3)	2.7 (3)	0.72 (1)
333	39.06	9.31 (4)	2.3 (4)	
373	37.13	12.69 (5)	1.3 (2)	0.59 (1)
440	34.03	19.89 (7)	1.2 (3)	
473	32.57	24.68 (8)	1.0 (2)	0.459 (6)

Table 2. Self-diffusion coefficients and shear viscosity of the mixture ammonia + methanol from present NVT simulations. The density was chosen to yield a pressure of 10 MPa. The number in parentheses indicates the statistical uncertainty in the last digit.

x_{NH3}	ρ	D_{NH3}	D_{MeOH}	η
mol mol^{-1}	mol L^{-1}	10^{-9} m^2 s^{-1}	10^{-9} m^2 s^{-1}	10^{-4}Pa s
243 K				
0	26.34		0.761 (6)	15 (1)
0.04	26.77	1.58 (4)	0.757 (6)	16 (1)
0.15	27.71	1.97 (2)	0.929 (8)	11 (1)
0.30	29.25	2.44 (2)	1.15 (1)	9 (1)
0.56	32.45	3.45 (3)	1.88 (2)	6.5 (7)
0.76	35.46	4.16 (3)	2.57 (3)	4.5 (6)
0.92	38.32	4.84 (3)	3.18 (5)	3.6 (5)
0.99	39.69	5.28 (3)	3.4 (2)	3.0 (4)
1	40.32	5.34 (3)		2.8 (3)
298 K				
0	24.78		2.41 (1)	5.7 (5)
0.04	25.05	4.78 (8)	2.43 (1)	5.2 (5)
0.15	25.91	5.32 (5)	2.93 (2)	4.9 (5)
0.30	27.18	6.33 (4)	3.64 (2)	3.7 (4)
0.56	29.91	7.80 (5)	4.71 (3)	2.9 (4)
0.76	32.11	9.57 (5)	6.28 (5)	1.9 (3)
0.92	34.30	10.84 (5)	7.5 (1)	1.6 (3)
0.99	35.42	11.45 (5)	7.8 (3)	1.3 (3)
1	35.87	11.60 (4)		1.5 (2)
373 K				
0	22.48		7.37 (3)	2.4 (2)
0.04	22.61	12.3 (2)	7.75 (3)	2.2 (3)
0.15	23.17	13.18 (9)	8.38 (4)	2.0 (3)
0.30	23.99	15.52 (8)	10.34 (5)	1.8 (2)
0.56	25.33	19.27 (9)	13.00 (9)	1.2 (2)
0.76	26.40	22.7 (1)	15.9 (1)	1.1 (2)
0.92	26.99	26.3 (1)	19.3 (2)	0.9 (2)
0.99	27.11	28.6 (1)	20.2 (4)	0.7 (2)
1	27.55	28.3 (1)		0.7 (1)

Table 3. Self-diffusion coefficients and shear viscosity of the mixture ammonia + methanol from present NVT simulations. The density was chosen to yield an average pressure of 100 MPa. The number in parentheses indicates the statistical uncertainty in the last digit.

x_{NH3}	ρ	D_{NH3}	D_{MeOH}	η
mol mol^{-1}	mol L^{-1}	10^{-9} m^2 s^{-1}	10^{-9} m^2 s^{-1}	10^{-4}Pa s
243 K				
0	27.65		0.481 (5)	24 (2)
0.04	28.11	1.01 (2)	0.477 (5)	23 (2)
0.15	29.13	1.36 (1)	0.679 (5)	18 (1)
0.30	30.76	1.74 (1)	0.923 (6)	14 (1)
0.56	34.71	2.57 (1)	1.46 (1)	9.1 (8)
0.76	37.26	3.34 (1)	2.09 (1)	6.4 (4)
0.92	40.25	3.93 (2)	2.67 (2)	4.5 (4)
0.99	41.71	4.39 (2)	3.04 (7)	3.2 (3)
1	42.31	4.11 (2)		3.4 (4)
298 K				
0	26.43		1.69 (1)	8.7 (7)
0.04	26.76	3.36 (5)	1.83 (1)	7.7 (6)
0.15	27.71	3.89 (3)	2.14 (1)	6.8 (5)
0.30	29.12	4.65 (2)	2.66 (1)	6.0 (6)
0.56	32.12	5.83 (2)	3.64 (2)	3.8 (4)
0.76	34.70	7.24 (2)	4.85 (3)	2.9 (3)
0.92	37.21	8.28 (3)	5.90 (5)	2.2 (2)
0.99	38.47	8.71 (3)	6.3 (2)	2.2 (2)
1	38.97	8.41 (3)		2.0 (2)
373 K				
0	24.75		5.17 (3)	3.4 (4)
0.04	24.98	8.72 (9)	5.47 (2)	3.1 (3)
0.15	25.75	9.57 (6)	6.08 (2)	2.9 (3)
0.30	26.91	10.71 (4)	6.97 (3)	2.5 (3)
0.56	29.16	13.05 (4)	8.98 (4)	1.9 (2)
0.76	31.16	14.96 (5)	10.72 (6)	1.8 (2)
0.92	33.00	16.67 (5)	12.31 (8)	1.4 (1)
0.99	33.89	17.33 (5)	12.8 (2)	1.3 (1)
1	34.41	16.80 (7)		1.1 (2)

Table 4. Self-diffusion and Maxwell-Stefan diffusion coefficients as well as shear viscosity of the mixture ammonia + methanol from present NVT simulations. The density was chosen to yield a pressure of 0.1 MPa. The number in parentheses indicates the statistical uncertainty in the last digit.

x_{NH3}	ρ	D_{NH3}	D_{MeOH}	$Đ_{ij}$	η
mol mol^{-1}	mol L^{-1}	10^{-9} m^2 s^{-1}	10^{-9} m^2 s^{-1}	10^{-9} m^2 s^{-1}	10^{-4} Pa s
293 K					
0.16	25.90	5.32 (4)	2.88 (2)	4.1 (6)	4.9 (6)
0.23	26.48	5.78 (4)	3.18 (2)	4.6 (7)	4.5 (4)
303 K					
0.16	25.55	6.16 (5)	3.43 (2)	5.4 (7)	4.2 (4)
0.23	26.10	6.68 (4)	3.75 (2)	6.6 (9)	3.9 (4)
313 K					
0.02	24.20	6.3 (2)	3.36 (2)	7 (1)	3.7 (4)
0.04	24.32	6.4 (1)	3.41 (2)	6.3 (9)	3.6 (4)
0.1	24.74	6.82 (6)	3.71 (2)	6.6 (8)	3.7 (4)
0.16	25.19	7.12 (6)	3.97 (2)	6.9 (9)	3.5 (2)
0.18	25.33	7.22 (5)	4.14 (2)	7.2 (8)	3.3 (4)
0.23	25.71	7.64 (5)	4.38 (3)	7 (1)	3.2 (2)

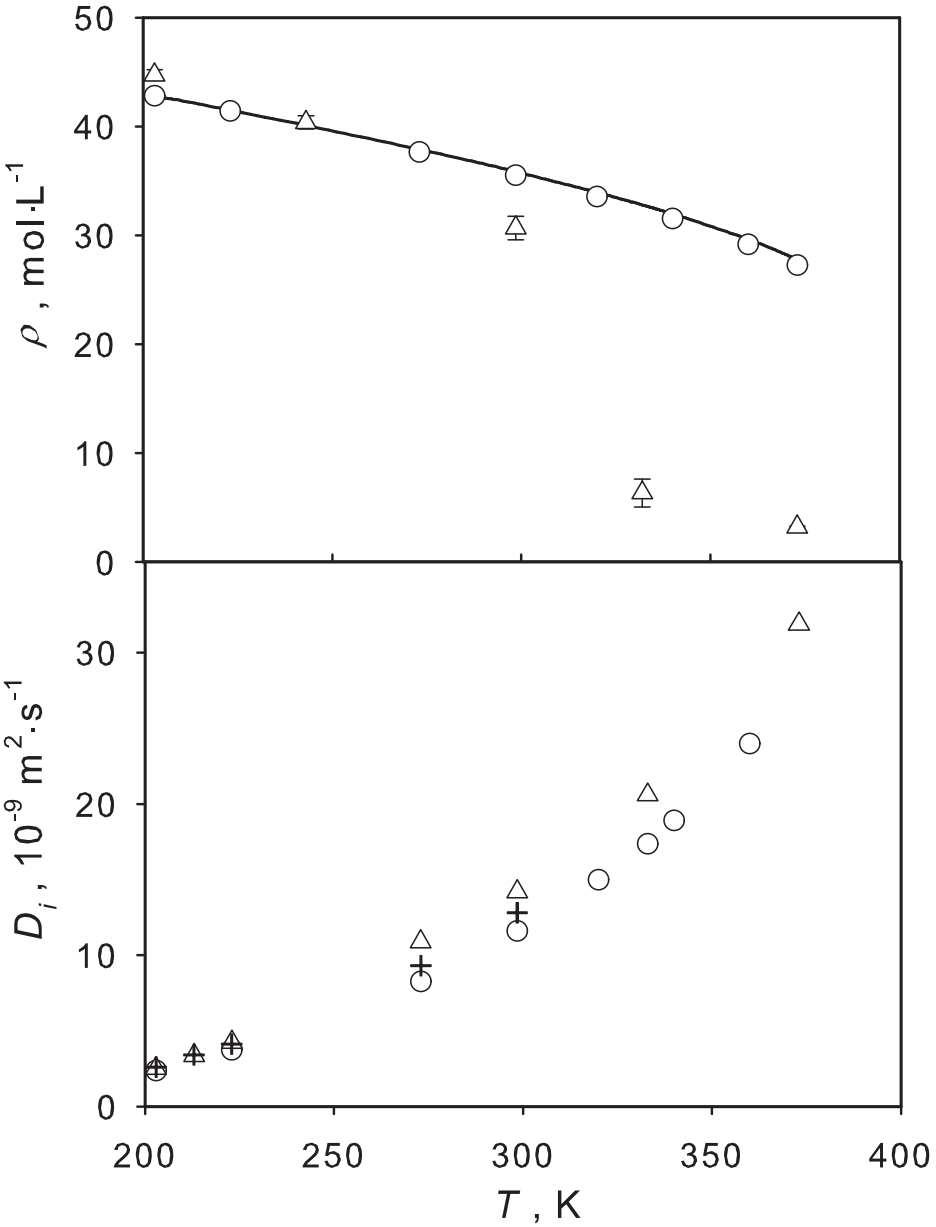

Figure 1. Top: Temperature dependence of the density of liquid ammonia at 10 MPa. The present predicted density (○) is compared to the simulation results based on OPLS−AA model modified by Feng et al. [1] (△) and the Helmholtz equation of state by Tillner-Roth et al. (–) [2]. Bottom: Temperature dependence of the self-diffusion coefficient of liquid ammonia at 10 MPa. Present simulation results (○) are compared to the simulation results by Feng et al. [1] (△) and to experimental data [3] (+). The statistical uncertainty of the present results is within symbol size.

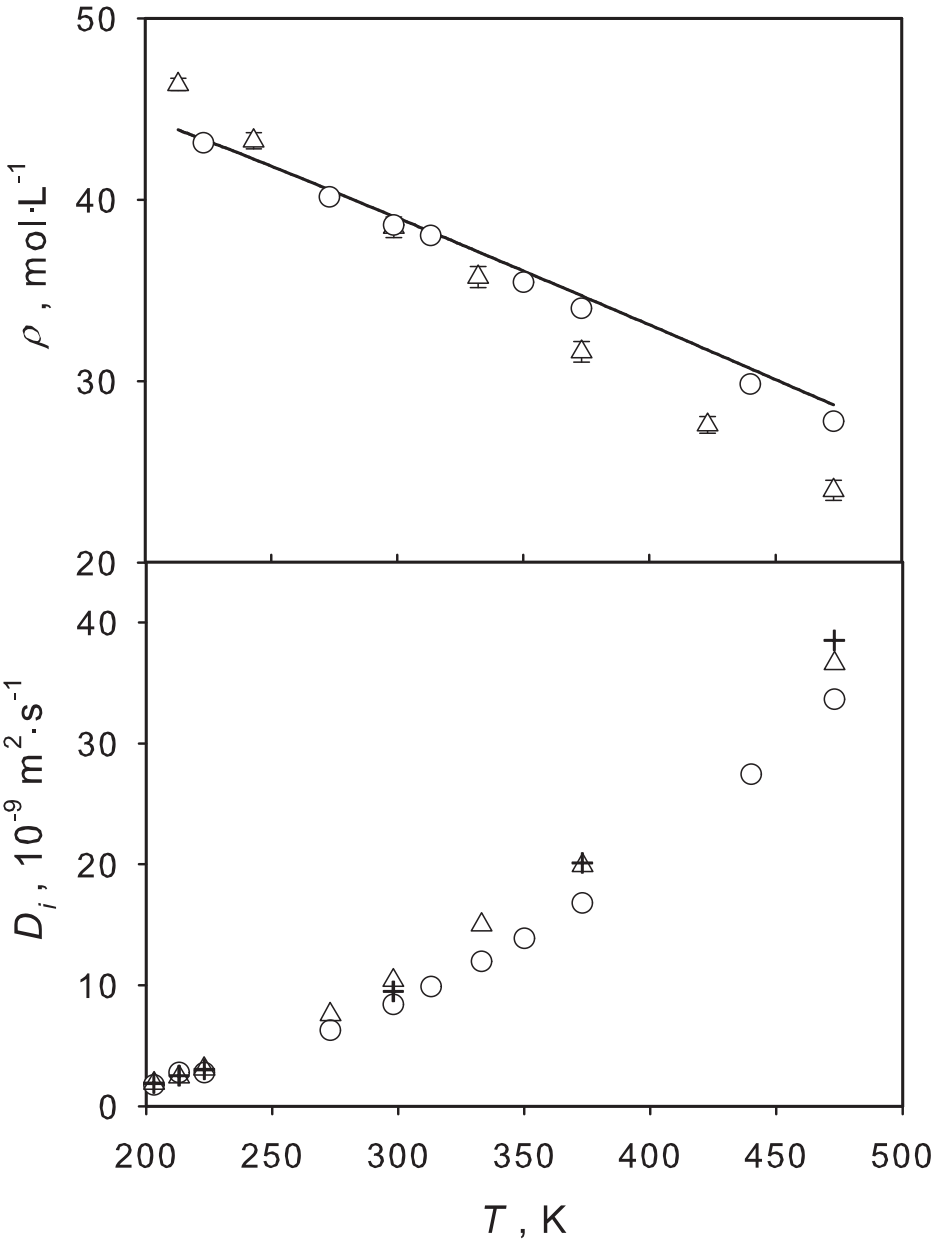

Figure 2. Top: Temperature dependence of the density of liquid ammonia at 100 MPa. The present predicted density (○) is compared to the simulation results based on the OPLS−AA model modified by Feng et al. [1] (△) and the Helmholtz equation of state by Tillner-Roth et al. (–) [2]. Bottom: Temperature dependence of the self-diffusion coefficient of liquid ammonia at 100 MPa. Present simulation results (○) are compared to the simulation results by Feng et al. [1] (△) and to experimental data [3] (+). The statistical uncertainty of the present results is within symbol size.

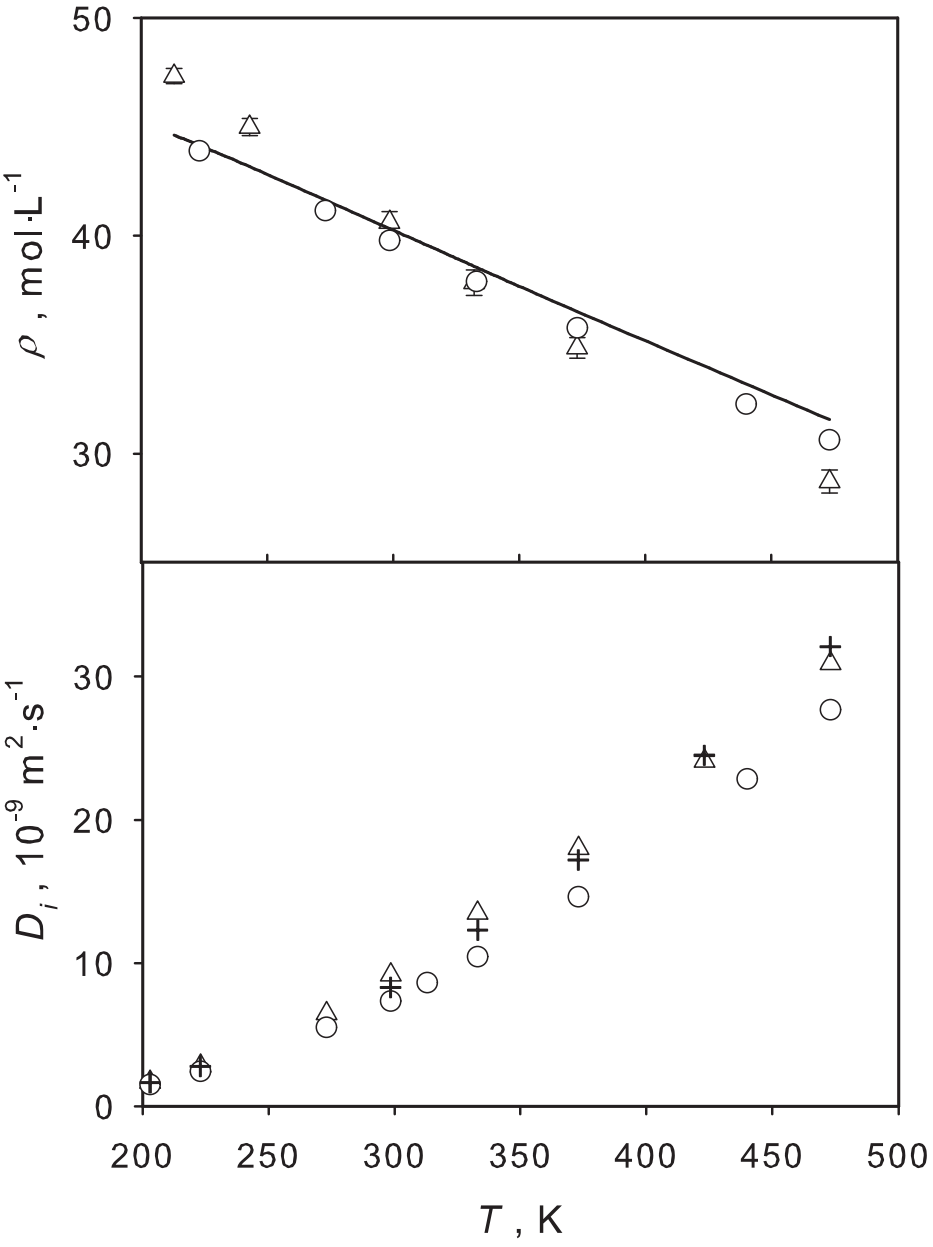

Figure 3. Top: Temperature dependence of the density of liquid ammonia at 150 MPa. The present predicted density (○) is compared to the simulation results based on the OPLS−AA model modified by Feng et al. [1] (△) and the Helmholtz equation of state by Tillner-Roth et al. (–) [2]. Bottom: Temperature dependence of the self-diffusion coefficient of liquid ammonia at 150 MPa. Present simulation results (○) are compared to the simulation results by Feng et al. [1] (△) and to experimental data [3] (+). The statistical uncertainty of the present results is within symbol size.

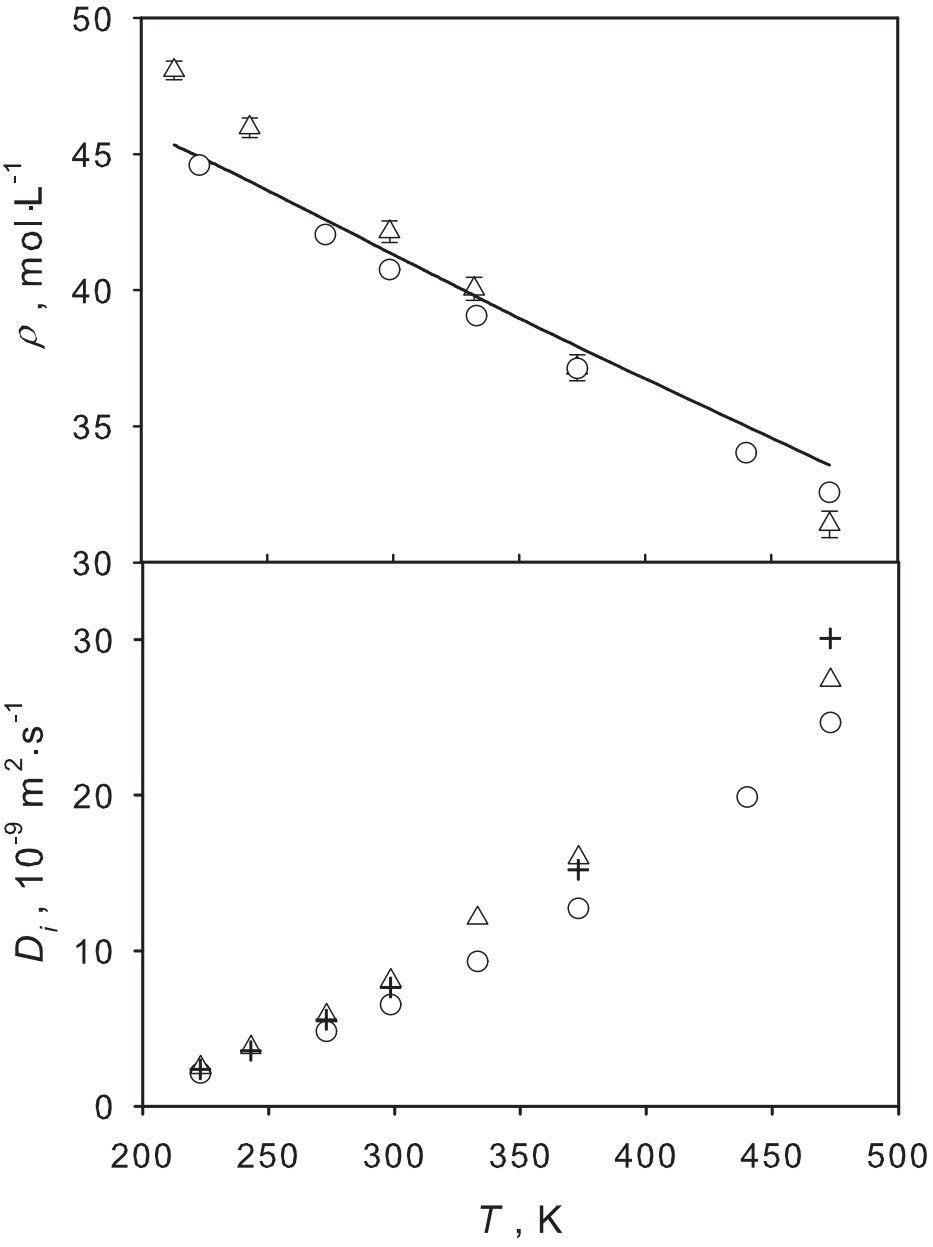

Figure 4. Top: Temperature dependence of the density of liquid ammonia at 200 MPa. The present predicted density (○) is compared to the simulation results based on the OPLS−AA model modified by Feng et al. [1] (△) and the Helmholtz equation of state by Tillner-Roth et al. (–) [2] . Bottom: Temperature dependence of the self-diffusion coefficient of liquid ammonia at 200 MPa. Present simulation results (○) are compared to the simulation results by Feng et al. [1] (△) and to experimental data [3] (+). The statistical uncertainty of the present results is within symbol size.

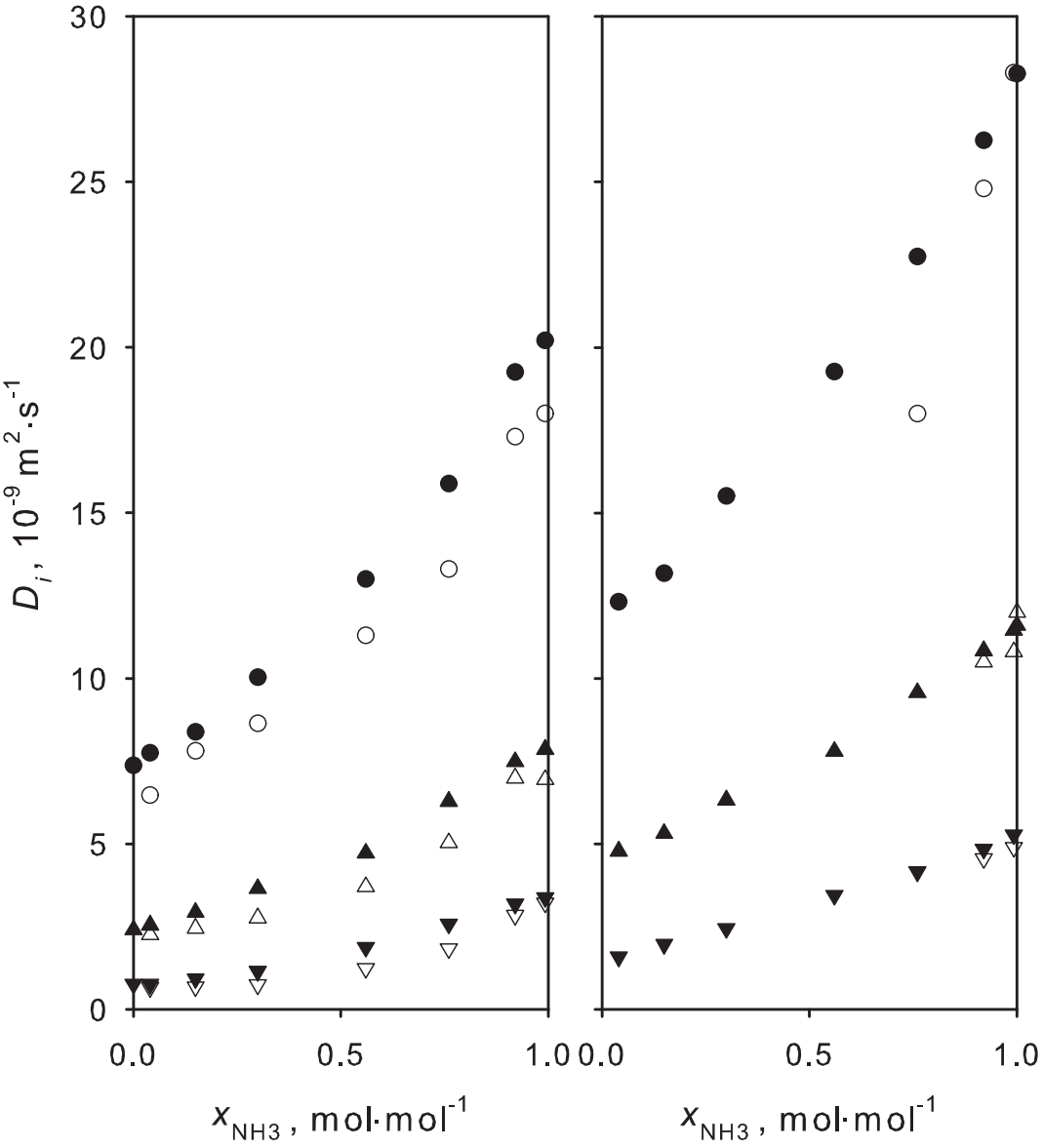

Figure 5. Composition dependence of the self-diffusion coefficients of ammonia (right) and methanol (left) in their binary mixture at 10 MPa. Present simulation results at 243 (▼), 298 (▲), and 373 K (●) are compared to experimental data [4] (open symbols). The statistical uncertainty of present results is within symbol size.

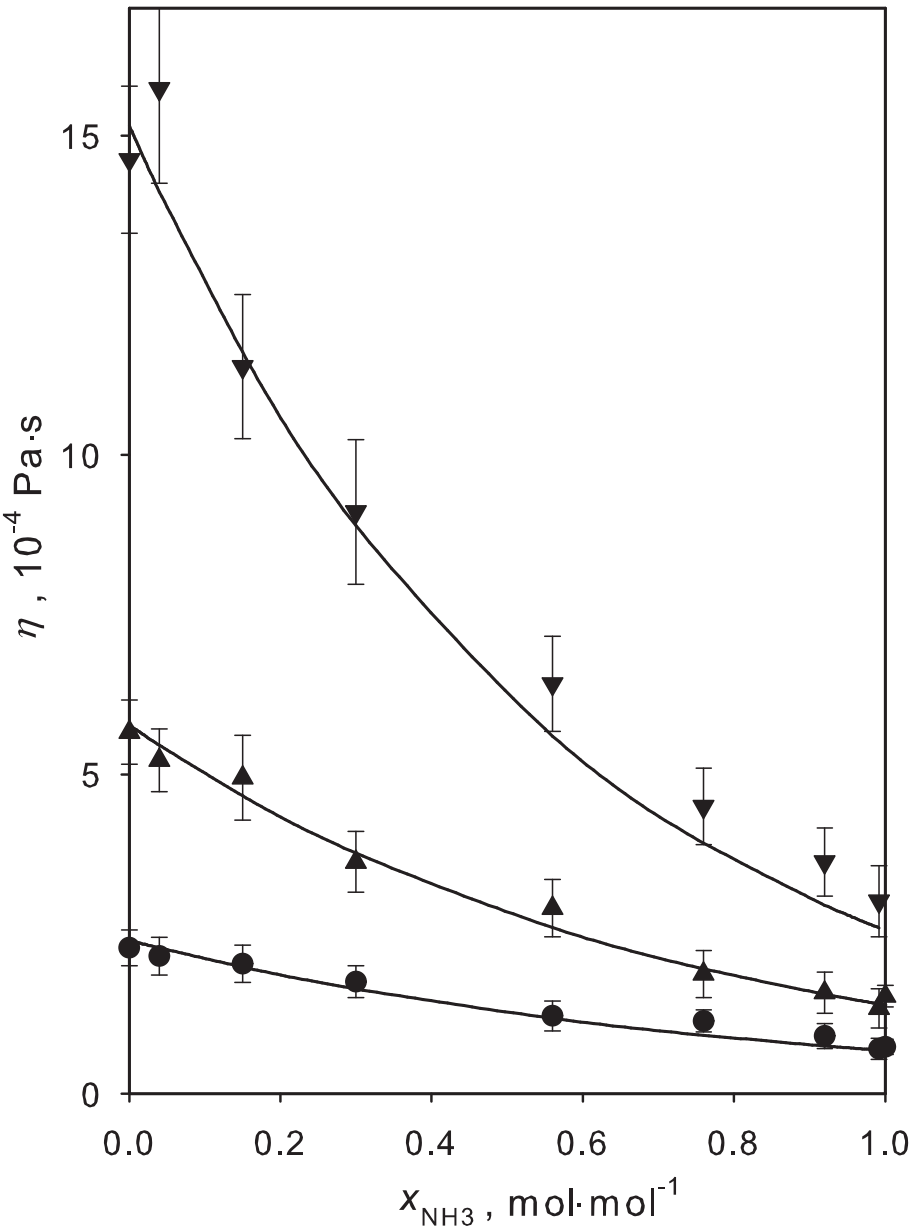

Figure 6. Composition dependence of the shear viscosity of the liquid mixture ammonia + methanol at 10 MPa. Present simulation results at 373 (•), 298 (▲), and 243 K (▼) are compared to the ideal solution shear viscosity (−), based on correlations of experimental data for the pure components [5,6]. The error bars indicate the statistical uncertainty only.

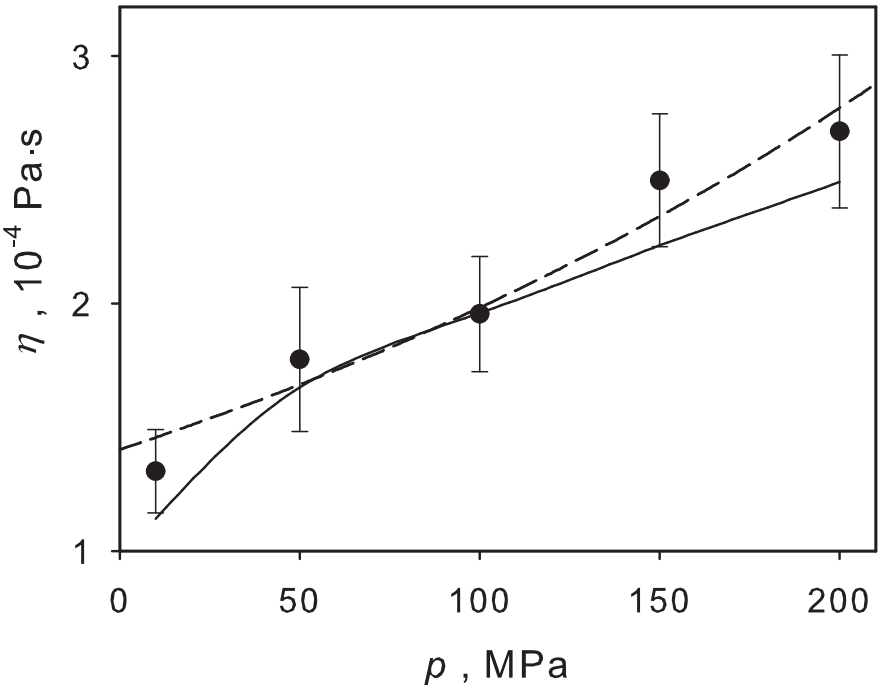

Figure 7. Pressure dependence of the shear viscosity of liquid ammonia at 298.5 K. The Barus model (−−) fitted to the present simulation results (•) is shown together with the correlation of experimental data by Fenghour et al. [5] (−). The error bars indicate the statistical uncertainty only.

Bibliography

[1] H. Feng, X. Liu, W. Gao, X. Chen, J. Wang, L. Chen, H.-D. Lüdemann, *Phys. Chem. Chem. Phys.* **12**, 15007 (2010)

[2] R. Tilner-Roth, F. Harms-Watzenberg, H.D. Baehr, *DKV-Tagungsbericht* **20**, 167 (1993)

[3] T. Gross, J. Buchhauser, W. Price, I.N. Tarasov, H.-D. Lüdemann, *J. Mol. Liq.* **73**, 433 (1997)

[4] T. Gross, L. Chen, J. Buchhauser, H.-D. Lüdemann, *Phys. Chem. Chem. Phys.* **3**, 3701 (2001)

[5] A. Fenghour, W.A. Wakeham, V. Vesovic, J.T.R. Watson, J. Millat, E. Vogel, *J. Phys. Chem. Ref. Data* **24**, 1649 (1995)

[6] H.W. Xiang, A. Laesecke, M.L. Huber, *J. Phys. Chem. Ref. Data* **35**, 1597 (2006)